https://dx.doi.org/10.1016/j.jcsr.2019.04.043

Design of CFRP-Strengthened Stainless Steel Tubular Sections subjected to Web Crippling

S. M. Zahurul Islam [a], Yancheng Cai [b,*] and Ben Young [c]

[a] *Department of Civil Engineering, Rajshahi University of Engineering & Technology, Rajshahi-6204, Bangladesh*

[b] *Department of Civil Engineering, The University of Hong Kong, Pokfulam Road, Hong Kong*

[c] *Department of Civil and Environmental Engineering, The Hong Kong Polytechnic University, Hong Kong*

(*Formerly, Department of Civil Engineering, The University of Hong Kong, Pokfulam Road, Hong Kong*)

Abstract: This paper presents a nonlinear finite element analysis and also depicts the design of stainless steel hollow square and rectangular sections strengthened by CFRP under web crippling loading configurations. Current design rules do not provide sufficient information for predicting the performance of CFRP-strengthened stainless steel hollow sections against web crippling. To develop a new comprehensive design rule, this research provided a nonlinear finite element analysis (FEA) based on a series of laboratory tests. The tests were conducted subjected to four different loading conditions, end-two-flange (ETF), end-one-flange (EOF) interior-two-flange (ITF) and interior-one-flange (IOF). Geometric and material nonlinear finite-element models were developed, substantiated by the experimental results. The traction separation law was used to simulate the debonding mechanism between the CFRP plate and stainless steel tubes in the nonlinear analysis process for the cohesive zone modeling. The finite-element models explicated well the behavior of CFRP strengthening and closely predicted the ultimate load-carrying capacity, web-crippling failure modes, as well as web-deformation curves of the tested sections. A parametric investigation was conducted using the verified finite element models for tubular sections with different dimensions. For CFRP enhancement of stainless steel members, the validated finite element models has been demonstrated as an constructive and time-saving method to determine the strengths of web crippling. The proposed design equation predictions also agreed well with the tests and numerical results. The web crippling strengths can be predicted effectively by the proposed design equation for CFRP enrichment stainless steel hollow sections against web crippling loading configurations.

Keywords: CFRP strengthening; Finite element analysis, Proposed design equation; Stainless steel; Tubular sections; Web crippling.

*Corresponding author. Tel.: +852 2859 2665; E-mail address: yccai@hku.hk (Y. Cai)

1. Introduction

The uses of cold-form stainless steel tubular structures have been rising recently due to different attractive advantageous features such as: corrosion resistance, durability, high strength-to-weight ratio, ease and speed of transportation, construction, and maintenance, fire resistance, nice look and recyclability of the material. Chromium and nickel are the two significant alloy-elements in stainless steels, as these deliver the basic corrosion-resistance and brightness of stainless steel members [1-2]. It is well established that the mechanical properties of carbon steel are not same as those of stainless steel. For carbon steel, the proportional limit is at least 70% of the yield strength, whereas it is 36% to 60% for stainless steel [3]. Cold-form tubular steel members are made up thin sheet steels which may buckle due to high slenderness ratio. For web crippling strength and behavior, many experimental investigations have been conducted on carbon steel since the 1940s [4-8]. The web crippling of thin-walled sections which also include hat sections have been investigated numerically [9-12]. The analytical and theoretical models for buckling of thin-walled members have been developed by many researchers [8, 10, 13-14]. Web crippling is a regular and major failure mode of thin–walled sections due to concentrated loads. The web crippling failure mode is often found in aluminum and cold-formed steel thin-walled members; this has been studied extensively [15-18]. Carbon fibre-reinforced polymers (CFRP) are able to improve the performance of steel structural members in terms of load-carrying capacity, stiffness, durability, strength-to-weight ratio and fatigue behavior [19]. Therefore, CFRP can be considered as an alternative solution to enhance web crippling strength for thin–walled sections.

Tests of CFRP-strengthened cold-formed stainless steel hollow sections have been conducted by Islam and Young [20-21] recently under web crippling loading. The test results revealed that the strengthening technique of CFRP had enhanced the load-carrying capacity by 51% and 76% for ferritic and lean duplex stainless steel respectively. This CFRP strengthening technique has provided a significant enrichment in web crippling load carrying capacity. Finite element analyses (FEA) were carried out by different researchers to investigate CFRP-strengthened metallic systems [22-28]. ABAQUS, the nonlinear finite element (FE) software, is used extensively to analyze diverse structural engineering problems; this software also includes simulations of system strengthened by CFRP [22-25, 28]. In terms of the FE analysis

of CFRP strength enhanced stainless steel hollow sections subjected to four web crippling loading configurations, the previous research is very limited and nothing has been found.

The current American Society of Civil Engineers Specification [29-30] and Australian/New Zealand Standard [31] for the design of cold-formed stainless steel structural members and European Code design [32-33] contain the web crippling design rules for bare carbon steel and stainless steel, respectively. This specified web crippling strength computing rule may not be implemented for the CFRP-strengthened stainless steel sections. A design model for web buckling strength computation of steel and aluminum was proposed by Zhao *et al*. [34] and Wu *et al*. [22] based on AS 4100 [35] for the strengthening of carbon steel RHS members under end loading condition. This design model was reformed by Fernando et al. [25] using two reduction factors. However, this design model is not appropriate for end-two-flange (ETF), end-one-flange (EOF) interior-two-flange (ITF) and interior-one-flange (IOF) loading conditions. So, there is a need to develop a unified design model that is more sophisticated and consistent based on a large database for CFRP strengthened stainless steel tubular sections against web crippling loading.

A series of tests on CFRP strengthening of ferritic and lean duplex stainless steel tubular members to enhance the web buckling capacity has been conducted by Islam and Young [20-21]. This research consisted of three phases (i) to develop accurate non-linear finite element models of CFRP strengthened stainless steel tubular structural members subjected to ETF, EOF ITF and IOF loading configurations using finite element program ABAQUS [36]; (ii) to conduct an extensive parametric study using verified FEM models for a broad range of hollow sections dimensions that having the web slenderness (h/t) 4.8 to 113.6; (iii) to develop a unified comprehensive design equation for CFRP strengthened stainless steel tubular sections against web buckling loading. The reliability of these proposed design rules is assessed by reliability analysis.

2. Experimental observations

An extensive test program on CFRP strengthening of web crippling of tubular sections was conducted by Islam and Young [20] for ferritic stainless steel as well as Islam and Young [21] for lean duplex stainless steel material under different loading configurations, such as, ETF,

ITF, EOF and IOF. A total of 75 specimens were tested, 37 of these were ferritic stainless steel and 38 were lean duplex stainless steel specimens including repeated tests. Fig. 1 presents the cross-sectional geometry and symbolic description of the square and rectangular hollow specimens. The parameters of the specimens were varied, including nominal thicknesses (t) from 1.5 to 4 mm; web depths (d) from 30 to 150 mm; flange widths (b) from 30 to 150 mm; measured web slenderness (h/t) from 8.1 to 57.3.In addition, the inner corner radius varies from 2.75 to 4.0 mm for ferritic stainless steel, and from 1.0 to 2.5 mm for lean duplex stainless steel sections. Under the following ETF, ITF and IOF loading configurations, the bearing length (N) was 50 mm. On the other hand, under the EOF loading configuration, the bearing length was 30 mm.

The material properties of the stainless steel tubular sections were obtained by tensile coupon tests according to ASTM [37] and AS [38] standards. Islam and Young [20-21] had conducted research experimentally to find best performance of FRP and adhesive on stainless steel. Islam and Young [20-21] have been presented properties of six different types of FRP and adhesive which was symbolized as 'a' to 'f' and 'A to 'F', respectively. The stress-strain curves of typical stainless steel and FRP are shown in Fig. 2. In this research, Sika CarboDur H514 laminate plate and Araldite 2015; and Sika CarboDur S1214 laminate plate and Araldite 420 was used which was provided best performance for strengthening the ferritic and lean duplex stainless steel tubular sections, respectively [20-21].

The sander and electric grinder surface treatment provide better performance for ferritic and lean duplex stainless steel tubular sections in terms of peak load enhancement, respectively [20-21]. Therefore, the sander and electric grinder surface treatment were used in this study for ferritic and lean duplex stainless steel tubular sections respectively. In Tables 1-22, specimens were labeled to easily identify material type, section geometry, the loading condition, type and number of CFRP layer which was described in details in Islam and Young [20-21].

For cold-formed stainless steel tubular section, the web crippling tests were performed in an INSTRON servo-controlled hydraulic testing machine. The tests were conducted by ETF, ITF, EOF and IOF loading conditions, as those specified in NAS and AS/NZS specifications [39-40], as shown in Fig. 3. For the ETF and ITF loading conditions, the load is applied at both top and bottom flanges of the sections, with the critical failure regions illustrated by the dotted lines, as shown in Figs. 3(a)-(b), respectively; while for the EOF and IOF loading conditions,

the load is applied at one flange of the sections with the critical failure regions illustrated by the dotted lines, as shown in Figs. 3(c)-(d), respectively. Details of the test setup and procedure are described by Islam and Young [20].

There are different failure modes of CFRP strengthened specimen are observed in experimental work in Islam and Young [20-21]. It was observed that the webs were buckled outward. Plastic hinge zone was formed in the middle of the webs in the ultimate limit state. In Tables 1–6, the web crippling loads per web (P_{Exp}) obtained from the tests for ferritic and lean duplex stainless steel sections are presented. For lean duplex, only the loading conditions for EOF and IOF are presented in this paper, as the loading conditions for ETF and ITF were presented by Islam and Young [21].

3. Finite element simulations

3.1 Finite element models

Finite element simulation has been used as a cost-effective complementary method to laboratory work. The finite element method (FEM) could be used as it is time saving, a powerful versatile solution technique and allows for extensive parametric study where the testing scope is limited. FEM attempts have been made by different researchers to investigate CFRP strengthened systems [22-23, 25-28]. Finite element models have been developed using the commercial software package ABAQUS [36] version 6.9-1.3D Finite Element (FE) models were built to simulate and compare with the experimental program. In the case of CFRP strengthening under web crippling configuration, it was necessary to model five key components accurately. These components are the bearing plates, stainless tubular section, adhesive, CFRP and the interfaces between stainless steel and adhesive; as well as the interfaces between the adhesive and CFRP plate. For simulation of the adhesive response using ABAQUS software, a cohesive element was used that followed traction separation law. In order to simulate and analyses the FE, the stainless section was modeled using a reduced integration 4-node doubly curved thin shell element. The S4R element is suitable for complex buckling behavior which has six degrees of freedom per node [36]. Thus, the interactions of bearing-stainless steel tube interfaces were defined as “surface-to-surface” contacts, with the bearings as master surfaces and the stainless steel tube top and bottom surfaces as slave counterparts.

For accurate results and less computational time, different mesh sizes for tubular cross-sections were investigated in the models. To achieve an appropriate meshing in FE modeling, a mesh convergence study was conducted. It was found that good simulation results could be obtained by using the element dimension varying from 2×2 (length × width in mm) to 10×10, which depends on the dimensions of the flanges and webs in a particular section. Appropriate meshing was obtained by trying some different meshes until mesh was fine enough; in the case of further mesh refinement there was no change in the ultimate load prediction. The corner region of tubular stainless steel section was modeled by dense meshing as shown in Fig 4. In this research, the mesh was converged by adapting accurate mesh in the FE models; the mesh-convergences details are available in Ref. [36]. As described in [20] and [21], measured initial geometric imperfections were deployed in this model.

In order to be able to make meaningful comparisons between numerical and experimental results, it is essential to ensure an adequate modelling of the member end support conditions. The boundary condition of the top bearing plate was simulated as a test condition by permitting the translational degree of freedom in the Y (vertical) direction and restraining against all other degrees of freedom. The nodal displacement in the X direction and rotation about the Y and Z-axis were prevented for the symmetry of the section. A symmetric boundary condition was applied to the stainless steel section against the section symmetric vertical axis. The discrete rigid 3D solid elements were used for modeling of the bearing plates. The bearing plate was simulated by 50×50×200 in mm volumetric rigid steel materials. The "contact pair" option was provided for modeling the interfaces between the bearing plates and the stainless section. The interaction between the bearing plate and the steel tube were modeled using the "surface to surface contact" in ABAQUS software. In terms of the finite element analysis, the rigid steel bearing plates were treated as the master elements; on the other hand, for the stainless specimen the slave element of the interface elements was stressed. The tie interface elements were used for the interface between stainless steel tube and adhesive, and adhesive-CFRP. It was ensured that the penetration between each of these was prevented in FE modeling. The nonlinear geometry parameter (*NLGEOM) was used in the analysis.

Vertical compression load was applied on the reference point of analytical rigid bearing plate through specifying displacement control. The (*STATIC) method which is available in the ABAQUS library was used to apply the incremental vertical load. The loading method of displacement control technique in the FEA was the same as that of the testing of the specimen,

where the specified value of 5 mm was generally used for the displacement. The details for the FE modeling procedure are described by Islam and Young [23].

3.2 Material model

The material properties of the stainless steel sections and adhesive were obtained from the tensile coupon tests. The coupon specimens were prepared and tested according to the international standards [37-38]. For ferritic stainless steel, the 0.2% proof (yield) stress ($f_{0.2}$) was varied 430-504 MPa, while ultimate tensile strength (f_u)varied 446-514 MPa, exponent parameter (n) value varied 4.8-6.4, tensile strain (ε_f) varied 10.0-21% and modulus of elasticity (E_o) varied 199.1-204.3 GPa. Similarly, for lean duplex stainless, the $f_{0.2}$ was varied 595-774 MPa, while (f_u) varied 733-861 MPa, exponent parameter (n) value varied 4.9-7.6, tensile strain (ε_f) varied 17.7- 38.7% and modulus of elasticity (E_o) varied 191.1-203.4 GPa.

The stress–strain curves of materials which were obtained by testing are used in the FEA. In order to simulate the material behavior in ABAQUS, the multi-linear stress–strain curve was used. The elastic part up to the proportional limit stress is represented by the first part of the multi-linear curve using the measured Young's modulus as well as a Poisson's ratio of 0.3. In order to carry out a large inelastic strains post buckling analysis, the conversion was performed for true stress and the logarithmic plastic strain curve from static engineering stress–strain curve. In ABAQUS [36], the equations related to the true stress (σ_{true}) and plastic true strain (ε_{true}^{pl}) true have been described in detail. The stress–strain curves present the material nonlinear behavior, including the computation of true stresses and logarithmic strains. The computation of true stresses and logarithmic strains are performed as follows:

$$\sigma_{true} = \sigma\,(1+\varepsilon) \tag{1}$$

$$\varepsilon_{true} = \ln\,(1+\varepsilon) \tag{2}$$

$$\varepsilon_{true}^{pl} = \ln\,(1+\varepsilon) - \sigma_{true}/E_o \tag{3}$$

where, E_o, σ *and* ε indicate their usual meanings, namely initial Young's modulus, stress and strain, respectively. Due to the cold working process, the strength of the corner material of the stainless steel tubular section was affected. Generally, the yield stress of corner material

properties is enhanced by approximately 50% compared to the flat material. Yuner and Young [41] conducted coupon test for corner material strength of lean duplex stainless steel specimens which were also incorporated in this FEM modeling; while for ferritic stainless steel, the yield stress of the corner material used 1.5 times of the flat coupon test results [20] and incorporated in the finite element model of this study.

Based on the test results for CFRP strengthening the ferritic and lean duplex stainless steel tubular sections, no other CFRP performance was as good as Sika CarboDur H514 and Sika CarboDur S1214 laminate plate, respectively [20-21]. Sika CarboDur H514 had the nominal modulus of elasticity of 300 GPa, ultimate tensile strength of 1500 MPa, tensile strain at fracture of 0.45% and thickness of 1.4 mm. The CFRP CarboDur S1214 laminate plate had the ultimate tensile strength of 3100 MPa, the nominal modulus of elasticity of 165GPa, tensile strain at fracture of 1.70% and thickness of 1.4 mm. The symbols 'f' and 'd' are used for CFRP of CarboDur S1214 and Sika CarboDur H514 laminate plate, respectively. According to the mill certificate from the supplier, the material behavior of CFRP was considered as a linear elastic material with elastic modulus 210 GPa as well as 300 GPa and thickness 1.4 mm. In the FE model, the S4R shell element was deployed for CFRP modeling using an assumed Poissons's ratio = 0.33.

An experimental investigation by Islam and Young [20-21] reported that adhesive Araldite 2015 and Araldite 420 showed the most excellent strength enhancement characteristics for ferritic and lean duplex stainless steel tubular sections, respectively, against compressive loading configurations. Material properties of adhesive Araldite 2015 and 420 were achieved by testing the tensile coupon [24]. Adhesive araldite 2015 had an ultimate tensile strength of 19.7 MPa, tensile strain at fracture of 3.3% and modulus of elasticity of 1.8 GPa. On the other hand, adhesive araldite 420 had an ultimate tensile strength of 24.3 MPa, tensile strain at fracture of 3.2% and modulus of elasticity of 1.6 GPa. In the finite element model for CFRP-strengthened stainless steel tubular sections, the adhesive response was simulated using a special cohesive element in ABAQUS [36]. Cohesive elements are useful and effective in modeling adhesives and bonded interfaces. The ABAQUS theory manual [36], Diehl [42] and Campilho *et al*. [43] detailed the performance of cohesive element, law of Traction-separation, and propagation of crack in adhesive layers. Hence, the cohesive element COH3D8 [36], namely, the 8-node three dimensional cohesive elements were used to model the adhesive layer.

The interface between the adhesive surfaces and the surface of the stainless steel tube was connected by tie constraints. The damage behavior of the adhesive layer was followed by the cohesive law. The law of traction-separation was considered for the cohesive elements to capture the initiation of damage. The traction-separation debonding performance was treated as bi-linear for the epoxy resin. In order to carry out adhesive modeling in FEA, the controlling properties of the traction-separation law have been included. The commercial FE program ABAQUS [36] was used in the modeling of the cohesive zone. The cohesive element was adopted in the FE models and the constitutive performance was characterized by the cohesive law of mixed-mode.

Measured tensile stress-strain behavior of the adhesive was adopted to describe the models of the bond-separation in this FE work. The tensile strength of the adhesive was treated as the peak stress of the bond-separation model. The debonding that happened during entire failure is occurred which was the result of the tensile strain at entire collapse and the glue thickness [36]. There are three components of bond stress which were incorporated into FEA and followed the mixed-mode cohesive law. Not only the normal stress component but also interfacial stresses bond stresses were deployed in the present study. The starting of the fracture of epoxy resin was defined by the strength criteria. The other properties of the stainless steel tubes, adhesive and CFRP materials were also used for the FEA models.

The cohesive elements provided by ABAQUS were adopted and their constitutive behavior was defined by the mixed-mode cohesive law. The elastic behavior was defined using the command *elastic, type = traction. The damage initiation behavior was defined using the command *damage initiation, criterion = QUADS. The damage evolution behavior was defined using the command *damage evolution, type = ENERGY, mixed mode behavior r = power law, power = 1. [36].

4. Verification of FE models

For validation purpose, FE models were calibrated against 66 web crippling test results on stainless steel tubular sections, including 34 ferritic and 32 lean duplex stainless steel specimens tested by Islam and Young [20-21]. It should be noted that the 9 repeated tests, including 3 for ferritic and 6 for lean duplex stainless steel specimens were not consider for

validation purpose. The repeated tests were conducted to ensure the reliability of the experimental results. It was found that the differences between the first and repeated test are small. Hence, the repeated test was not included for in the FE validation. The developed FE models include ETF, ITF, EOF and IOF loading configurations. Verification of FEM is needed due to calibration with tested results. The test results were compared with the FEM results in order to verify and check the accuracy of the FE. The finite element models were calibrated against the test results in terms of collapse type, web-buckling, deflection, and ultimate load-bearing capability.

The loading conditions are demonstrated on the collapse mode of the CFRP strengthened stainless steel tubular structural members against web crippling. The precise prediction of the web collapse type is very important in FE. The common failure mode of the CFRP-strengthened stainless steel tubular sections against web crippling was observed as debonding failure. The experimental progressive damage mode of the adhesive layer is shown in Fig. 5. Fig. 6 depicts the FEA progressive damage mode of the adhesive layer by FEA. It reports the collapse type and stress distribution on the adhesive layer for the stainless steel section F60×40×3-ETF-f1 at different loading stages. The comparisons of the experimental and FEA progressive failure mode of the CFRP-strengthened stainless steel sections are detailed in Figs.5-6. The Load ratio (R), which was the ratio of applied load (P) at particular stage to the maximum applied load (P_u or P_{FEA}), value of applied load (P), web deformation (Δ) and time (T) in second are presented in Figs. 5 and 6, for both the experimental investigation and FEA at different stages of loading. It was found that the collapse modes predicted by the FEA are in excellent match with those found in the experimental investigation. The failure modes resulting from different loading conditions of the strengthening technique are also represented closely by FEM.

The relative displacement of epoxy is governed the cohesive tractions properties which is followed constitutive law. According to Simulia ABAQUS [36], the constitutive law is stated as stress against equivalent displacement, rather than stress against strain. Under incremental compressive loading, the decohesions were propagated gradually in the damaging zone, which was simulated by the constitutive law in FEA. The fracture mode and stress distribution on adhesive layers under different loading levels was presented in previous research by Islam and Young [23]. Maximum Von Mises stress allocations for adhesive layers at low load level were depicted in earlier research. Due to low loading levels, maximum Von Mises stress was found

at the peak and underneath the corner edge of the epoxy layer. The previous research by Islam and Young [23] depicted the peak Von Mises stress at the upper and lower edges of epoxy layer due to progressively applied intermediate loading levels. Debonding failure is initiated when Von Misses stress attains the ultimate stress of epoxy. The earlier research [23] presented the starting debonding process with damage of the epoxy layer obtaining zero Von Mises stress. Potential failure mechanisms of the epoxy layer have been described by Islam and Young [23-24]. Fracture of the epoxy layer starts when the Von Misses stress attains the ultimate normal bonding stress limit. At a high load level, the maximum Von Mises stress was observed for the adhesive layer. In the FE simulation, the region of height Von Mises stress in the epoxy layer rose sharply with the rising of the load demonstrating progressive bond collapse as found in laboratory testing. A scalar fracture variable is initiated after the beginning of damage which is zero at the starting of damage and is one at complete failure [36]. Decohesion was developed slowly due to incremental loading and fractures propagated from either the top or bottom boundaries to the mid-portion of the web; this followed an identical trend as for experimental failure. Epoxy damage starting and progressive collapse types predicted by the FEA agree well with those observed experimentally. Figs. 7-11 depict the collapse type achieved experimentally on the CFRP-strengthened stainless steel sections which match the FE analysis evaluations for ETF, ITF EOF and IOF configurations, respectively. It can be concluded that the FEA predicted failure mode was found to be in good agreement with the experimental failure mode. The load vs web deformation curves achieved from these FEA models were calibrated with lab tested curves under ETF, EOF, ITF and IOF loading configurations, as shown in Figs. 11-14, respectively. In the elastic as well as the elastic–plastic phases, good agreement was found between the curves from the non-linear FE analysis and those obtained experimentally. It was observed that the prediction of web crippling strength and behavior was good enough by means of large strain nonlinear FEM analysis.

For the ETF, ITF, EOF and IOF loading configurations, Tables 1-6 shows the comparison of the experimental ultimate web crippling strengths per web (P_{Exp}) with those of FEA outcome (P_{FEA}) of ferritic and lean duplex stainless steel sections, respectively. In case of ferritic steel sections, mean ratios (P_{Exp}/P_{FEA}) of 1.03, 1.03, 1.02, and 1.03were achieved with the corresponding coefficient of variation (COV) of 0.041, 0.039, 0.042 and 0.054, respectively. One the other hand, for lean duplex stainless steel sections, mean ratios (P_{Exp}/P_{FEA}) of 1.04, and 0.99 were achieved with the corresponding coefficients of variation (COV) of 0.029 and 0.051, for EOF and IOF loading, respectively. For lean duplex, ETF and ITF loading conditions

were presented in previous publication of Islam and Young [21]. Excellent agreement was achieved between the FEA predictions and the experimental results for ferritic as well as lean duplex stainless steel sections.

5. Parametric investigation

5.1 Specimens

According to the validation, the structural strengthening and behavior of the CFRP-strengthened stainless steel hollow sections under four different web crippling loading conditions was predicted closely by the FEM. To examine the effects of the web slenderness ratio (*h/t*), different dimensional (thicknesses, sizes and cross-section) specimens were considered in these parametric investigations. In this parametric study, 48 ferritic and 56 lean duplex stainless steel specimens, in total 104 specimens, were used for the FE models analysis, having the variation of wide range key parameter. The ferritic and lean duplex stainless steel wide range square and rectangular specimens were analysed in the parametric study. Tables 7-10 and Tables 11-14 summarize the wide range of cross-sections as well as the web crippling strengths (P_{FEA}) per web predicted from the FEA under the four loading configurations for ferritic and lean duplex stainless steel, respectively. The properties of adhesive and CFRP (e.g. thickness, tensile strength Young's modulus) were included in the parametric study

In the parametric study, fifteen different dimensional sizes were considered which comprised web-depths of 35 to 200 mm; thicknesses of 1.6 to 4.5 mm; flange widths of 35 to 150 mm; and aspect *d/b* ratios of 1 to 4. Seven square (SHS) and eight rectangular(RHS) were included in this study, with varied dimensions from 35×35×4 to 200×100×1.8 in mm. The effects of the web slenderness ratio of stainless steel tubular sections due to the strengthening of CFRP against web crippling were the main focus of this parametric study. The web slenderness values ranged from 4.7 to 113.6. According to the Specification of American Society of Civil Engineers (ASCE) [29], the specimen lengths (L) were designed for the ETF, ITF, EOF and IOF loading configurations. Web depth (d), flat portion web depth (h), and the bearing length (N = 50 mm) were considered for specimen length calculation.For the EOF loading configuration, a reduced bearing length (N = 30 mm) and specimen length were used to keep away collapse at the mid-portion of the sample as shown in Table 9 and Table 13. For the

parametric investigations, the specimen labels were followed as the experimental program [20-21] as well as described in this paper in Section 2.

5.2 Parametric FE analysis

The material properties of the tested F80×80×3 and D100×50×2.5 sections were used in FEM for the analyses of the ferritic and lean duplex stainless sections, respectively [20-21]. The ferritic stainless steel section F80×80×3 had $f_{0.2}$ = 434 MPa, f_u = 461 MPa, n = 5.9, ε_f = 19.9% and E_o = 199.1 GPa. On the other hand, lean duplex stainless section D100×50×2.5 had $f_{0.2}$ = 606 MPa, f_u = 733 MPa, n = 7.5, ε_f = 37.6% and E_o = 202.7 GPa. The true stress (σ_{true}) as well as plastic true strain (ε_{true}^{pl}) of F80×80×3 and D100×50×2.5 sections, transformed from the tested static engineering stress-strain curve was used in the parametric study for ferritic and lean duplex stainless sections, respectively.

The meshing, boundary configurations and loading technique were adopted as similar to the calibrated FE models. Tables 7-10 and Tables 11-14 depict the ultimate web crippling strengths (P_{FEA}) per web obtained from the FEA for the ferritic and lean duplex stainless steel sections under ETF, ITF, EOF and IOF loading configurations, in that order. Table 7 and Table 11depict that the enrichment of the CFRP strengthening rise due to the web slenderness ratio rising up to 71.0 and 66.6 for ferritic and lean duplex stainless steel section, respectively. The CFRP strengthening of the ferritic section and the lean duplex steel consequence fell progressively while the web slenderness ratios went beyond 71.0 and 66.6, respectively. The ratios of *h/t*, *N/t*, r_i/t and *N/h* have a significant influenced on the strength of web crippling. It was found that the web slenderness ratios of 71.0 and 66.6 in the respective cases of ferritic and lean duplex stainless steel sections provided maximum strengthening performances. Therefore, it can be concluded that the CFRP strength enrichment rise when the web slenderness ratio also rise until a specific limit.

6. A**nalysis for reliability**

The relative measure of safety for the design equation is calibrated by safety index (β). The reliability analysis was included in this study to determine the reliability of the web crippling

design. The ASCE Specification [29] recommends a target reliability index of 3.0 for stainless steel structural members, which is at a lower limit [44]. The design equation was treated as a reliable measuring tools for this research, if the safety index was found to be larger than 2.5 (β > 2.5) due to CFRP strengthening. In the reliability analysis, the load combinations of 1.2DL+1.6LL, as stated in the American Society of Civil Engineers Standard [44], were used, where DL is the dead load and LL is the live load. For reliability analysis, a total of 170 results are presented that consist of 66 test results and 104 numerical results**.** The 170 results were used to propose design equation and for reliability analysis**.** According to NAS Specification [45] for web crippling strength, the value of statistical parameters are M_m = 1.10, F_m = 1.00, V_M = 0.10, and V_F = 0.05. The M_m, F_m, V_M and V_F are mean values and coefficients of variation for material properties and fabrication variables. Tables 15-18 and Tables 19-22 depict the statistical parameters of P_m and V_p of the tested-to-predicted load ratios for ferritic and lean duplex stainless steel sections for the four loading conditions, respectively

7. Proposed design equation (P_P)

Practicing engineers have strong desire and motivation to obtain a precise unique design rule for CFRP strengthened stainless steel tubular members. Current design rules are not able to compute the performance of CFRP strengthened stainless steel tubular segment under four different loading conditions. Hence, the web crippling design equation was proposed for CFRP strengthening of stainless steel tubular sections under ETF, ITF, EOF and IOF loading configurations. Previous investigations conducted by Zhou and Young [46-47] have shown that the web crippling strength and behavior of the stainless steel sections were affected by the primary parameters, such as t, f_y, r_i/t N/t and h/t. These parameters were reflected in the unified semi-empirical equation for web crippling strength specified in the NAS Specification [45]. However, this unified equation is suitable for the web crippling of stainless steel sections without CFRP strengthening. The investigation in the present study have shown that the web crippling strengths of CFRP-strengthened sections are significantly influenced by the bonded area, the property of adhesive and CFRP (e.g. thickness, tensile strength) for the ferritic and lean duplex stainless steel tubular sections. Hence, the mechanical properties of adhesives, debonding of the interface between the CFRP and stainless steel surface and the bonded area of the CFRP for the CFRP-strengthened specimens need to be considered in the design model.

To account for the above factors, an additional term for the effects of the CFRP-strengthening was proposed based on the unified equation specified in NAS Specification [45], as shown in Equation (4), which is in a similar manner as the equation proposed by Zahurul and Young [23] for CFRP-strengthened aluminium tubular sections.

$$P_p = Ct^2 f_y \sin\theta \left(1 - C_R\sqrt{\frac{r_i}{t}}\right)\left(1 + C_N\sqrt{\frac{N}{t}}\right)\left(1 - C_h\sqrt{\frac{h}{t}}\right) + [\sigma_{u-ad}.A_{bonding}].C_{ad-FRP} \quad (4)$$

where t = web thickness; C = coefficient; f_y = yield stress; N = bearing length; h = web depth; C_R = corner radius coefficient (inside); C_N = bearing length coefficient; C_h = web slenderness coefficient; σ_{u-ad} = ultimate tensile stress of adhesives, $A_{bonding}$ = FRP bonded area and $C_{ad\text{-}FRP}$ = coefficient of adhesive-FRP.

The proposed equation was developed based on a total of 177 results including the 73 (37 ferritic + 36 lean duplex) test results, and the 104 parametric results performed in the present study. It should be noted that the sections with and without CFRP strengthening were used, where the additional term for the effects of CFRP strengthening was not applicable for the sections without CFRP strengthening. The effects of the bonded area, ultimate stress of adhesive and coefficient of adhesive-CFRP for CFRP-strengthened stainless steel tubular members were incorporated in the Equation (4), by the $A_{bonding}$, σ_{u-ad} and $C_{ad\text{-}FRP}$, respectively. The values of the coefficients with the corresponding resistance factors for the equation were calibrated based on the aforementioned 177 results for the ferritic and lean duplex stainless steel tubular sections, as shown in Table 23. The limitations of the proposed coefficients for the different grades of stainless steel are also specified.

8. Calibration of design strengths (P_P) through experimental and numerical results

Tables 15-18 and Tables 19-22 compare the predicted design strengths (P_P) using the proposed design Equation (4) with the experimental and numerical ultimate web crippling strengths (P_{Exp} and P_{FEA}) of the ferritic and lean duplex stainless steel sections, respectively, under the ETF, ITF, EOF and IOF loading configurations. The measured cross-section dimensions and

material properties were used in the calculation of predicted strengths. For the case of the ferritic steel sections (See Tables 15-18), the mean values of 1.05, 1.01, 1.00 and 1.00 are achieved through the subsequent coefficients of variation (COV) of 0.155, 0.123, 0.111 and 0.072, and the corresponding reliability indices (β) of 2.52, 2.53, 2.53 and 2.71, correspondently. In the reliability analysis, the resistance factors ϕ_w = 0.85 for ETF, ITF, EOF and IOF loading configurations were used. For the case of lean duplex stainless steel sections (See Tables 19-22), the mean values of 1.03, 1.03, 1.04 and 1.00 were achieved through the subsequent COV of 0.176, 0.143, 0.144and 0.108, and the corresponding reliability indices (β) of 2.55, 2.52, 2.51 and 2.56. In the reliability analysis of lean duplex stainless steel, resistance factors (ϕ_w) of 0.80, 0.85, 0.85, and 0.85 were used for the corresponding ETF, ITF, EOF and IOF loading configurations.

Tables 15-18 and Tables 19-22 demonstrate that the proposed design rules are generally reliable and safe with the best use of material strength for predicting web crippling strength and that they compare well with the experimental and numerical results for the CFRP-strengthened ferritic and lean duplex stainless steel sections, respectively. The reliability indices (β) are larger than the specified value of 2.5 for ETF, ITF, EOF and IOF loading configuration. Therefore, the proposed design rules are found to be reliable for adhesive CFRP-strengthened stainless steel tubular sections under four loading configurations within the limiting values described in Table 23.

9. Conclusions

This paper has presented the development of numerical (nonlinear finite-element) models and proposed design equation for CFRP strengthened ferritic and lean duplex stainless steel tubular sections against web crippling. The FE models include geometric and material non-linearity. In terms of the collapse modes, web load-deformation curves and web-crippling strengths under different loading configurations like ETF, ITF, EOF and IOF, the FEA results have been verified with the experimental results. The traction-separation law was considered for the cohesive elements for simulating damage to the adhesive layer. In this research, the web crippling strengths and behavior of CFRP strengthening on webs of stainless steel tubular

hollow sections have been predicted closely using finite element analysis. Therefore, the calibrated finite-element models have been deployed to accomplish an extensive parametric study for a broad range of cross-sectional dimensions, and the web slenderness ranged from 4.7 to 113.6.This research had led to the proposal of unified web crippling design equation for stainless steel tubular sections that were CFRP-strengthened under the ETF, ITF, EOF and IOF loading configurations. The web crippling strengths anticipated by the tests and finite element analysis have been compared with the design strengths calculated using the proposed equation. A reliability analysis was performed and it was evident that web crippling strengths predicted by the proposed design equation gave an allowable safety margin. It was concluded that the web crippling strengths computed by means of the proposed design equation gave a safe and reliable design for CFRP-strengthened ferritic and lean duplex stainless steel tubular sections.

Acknowledgements

The authors are grateful to STALA Tube Finland for supplying the test specimens. The research work described in this paper was supported by a research grant from The University of Hong Kong under the seed funding program for basic research.

Nomenclature

The following symbols are used in this paper:

$A_{bonding}$ = CFRP bonded area;
b = flange width;
C = web crippling coefficient;
$C_{ad\text{-}FRP}$ = coefficient of adhesive-FRP;
C_h = web slenderness coefficient;
C_N = bearing length coefficient;
C_R = inside corner radius coefficient;

CFRP = Carbon Fibre-Reinforced Polymer;

COV = coefficient of variation;

DL = dead load;

d = overall depth of web;

E_o = initial Young's modulus;

F_m = mean value of fabrication factor;

FRP = Fibre-Reinforced Polymer;

h = depth of flat portion of web measured along the plane of web;

L = actual length of test specimen;

LL = Live load;

M_m = mean value of material factor;

N = length of bearing plate;

n = exponent in Ramberg-Osgood expression;

P = Applied Load in FEA;

P_{Exp} = experimental ultimate web crippling loads per web with CFRP;

P_{FEA} = web crippling strength predicted from finite element analysis, where the sections without CFRP-strengthening was distinguished by $P_{FEA,0}$ in the parametric study;

P_m = mean value of tested-to-predicted load ratio;

P_p = web crippling strength calculated using proposed unified equation;

R = load ratio between the applied load and the ultimate load of the section;

RHS = Rectangular Hollow Section;

r_i = inside corner radius;

SHS = Square Hollow Section;

t = thickness of stainless steel tube;

T = Time

V_F = coefficient of variation of fabrication factor

V_M = coefficient of variation of material factor

V_p = coefficient of variation of tested-to-predicted load ratio;

σ_{u-ad} = ultimate tensile stress of adhesives;

β = reliability index;

θ = angle between the plane of web and the plane of bearing surface;

ε_f = elongation (tensile strain) after fracture based on gauge length of 50 mm;

$f_{0.2}$ = static 0.2% tensile proof stress (yield strength);

f_y = yield stress;

f_u = static tensile strength;

Δ = web deformation;

ϕ_w = resistance (capacity) factor;

References

[1] Ashraf, M. Structural stainless steel design: resistance based on deformation capacity. PhD Thesis, Department of Civil and Environmental Engineering, Imperial College London, UK. 2006.

[2] Nilsson J.O, Chai G., Kivisäkk U. Recent development to stainless steels. In: Proceedings of the sixth European stainless steel conference. Finland; 2008, p.585–90.

[3] Yu, W.W. and LaBoube R.A. Cold-formed steel design, Fourth Edition, John Wiley and Sons, Inc., New Jersey. 2010.

[4] Zetlin, L. Elastic instability of flat plates subjected to partial edge loadings. *Journal of the Structural Division.* ASCE Proceedings, 1955, 81.

[5] Winter, G. and Pian, R.H.J. Crushing strength of thin steel webs. *Engineering Experiment Station, Bulletin No.35*, Cornell University, N.Y., U.S.A. 1946.

[6] Santaputra, C. Web crippling of high strength cold formed steel beams, Ph.D. Thesis, University of Missouri-Rolla, Rolla, Missouri, U.S.A. 1986.

[7] Studnicka J. Web crippling of multi-web deck sections, *Thin-Walled Structures*, 1991, 11, (3): 219-231.

[8] Bakker M. C. M. and Stark J. W.B., Theoretical and experimental research on web crippling of cold-formed flexural steel members, *Thin-Walled Structures*, 1994, 8,(4);261-290.

[9] Wiseman D. L, Puckett J.A. Applications of compound strip method for folded plates with connecting elements. *Journal of Structural Engineering* 1991,117(1):268–85.

[10] Davies J.M. and Jiang C. Design procedures for profiled metal sheeting and decking. Thin-Walled Structures, 1997, 27:43–53.

[11] Samanta A and Mukhopadhyay M. Finite element static and dynamic analyses of folded plates. *Engineering Structures*, 1999, 21:277–87.

[12] Hofmeyer, H. Cross-section crushing behaviour of hat-sections Part I: Numerical modeling, *Thin-Walled Structures*, 2005, 43 (8): 1143-1154.

[13] Park M.S. and Lee B.C. Prediction of mode parameters and moment-rotation curves for crushed thin-walled trapezoidal tubes in bending. *Journal of Applied Mechanics* 1996, 63:453–9.

[14] Macdonald, M., Don M.A H., KoteŁko, M. and Rhodes, J. Web crippling behaviour of thin-walled lipped channel beams, *Thin-Walled Structures*, 2011, 49(5): 682-690

[15] Young B. and Hancock G.J. Design of cold-formed channels subjected to web crippling. *Journal of Structural Engineering*, ASCE 2001, 127(10): 1137-1144.

[16] Young B. and Zhou F. Aluminum tubular sections subjected to web crippling—Part II: Proposed design equations. *Thin-Walled Structures*, 2008; 46(4): 352-361.

[17] Zhou F., Young B. and Zhao X.L. Tests and design of aluminum tubular sections subjected to concentrated bearing load. *Journal of Structural Engineering*, ASCE 2009, 135(7): 806-817.

[18] Islam S.M.Z. and Young B. FRP strengthened aluminium tubular sections subjected to web crippling, *Thin-Walled Structures*, 2011; 49(11):1392-1403.

[19] Zhao X.L. and Zhang L. State-of-the-art review on FRP strengthened steel structures. Engineering Structures 2007; 29(8):1808–1823.

[20] Islam S. M. Z. and Young B. Ferritic stainless steel tubular members strengthened with high modulus CFRP plate subjected to web crippling. Journal of constructional steel research, 2012; 77:107-18.

[21] Islam S. M. Z. and Young B. FRP strengthening of lean duplex stainless steel hollow sections subjected to web crippling. *Thin-Walled Structures*, 2014, 85: 183-200.

[22] Wu C., Zhao X.L., Duan W.H. and Phipat P. Experimental and numerical study on CFRP strengthened aluminium tubular sections subjected to end bearing force. *International Journal of Structural Stability and Dynamics*, 2012; 12(1).

[23] Islam S. M. Z. and Young B. Design of CFRP-Strengthened aluminium tubular sections subjected to web crippling. *Thin-Walled Structures*, 2018, 124: 605-621.

[24] Islam S. M. Z. Strengthening of aluminium and stainless steel tubular sections with Fibre-reinforced polymer. PhD Thesis, Department of Civil Engineering, The University of Hong Kong. Hong Kong, China, 2012.

[25] Fernando D., Yu T., Teng J.G. and Zhao X.L. CFRP strengthening of rectangular steel tubes subjected to end bearing loads: Effect of adhesive properties and finite element modelling. Thin-Walled Structures 2009; 47(10):1020-1028.

[26] Fawzia S., Al-Mahaidi R. and Zhao X. L. Experimental and finite element analysis of a double strap joint between steel plates and normal modulus CFRP, Composite Structures 2006; 75(1-4): 156-162.

[27] Zhang L.F. and Teng J. G. Finite element prediction of interfacial stresses in structural members bonded with a thin plate, Engineering Structures 2009; 32(2): 459-471.

[28] Silvestre N., Young B. and Camotim D. Non-linear behaviour and load-carrying capacity of CFRP-strengthened lipped channel steel columns. Engineering Structures 2008; 30(10):2613-2630.

[29] ASCE. Specification for the design of cold-formed stainless steel structural members. SEI/ASCE 8-02; Reston, VA: American Society of Civil Engineers; 2002.

[30] American Society of Civil Engineers. Commentary on Specification for the design of cold-formed stainless steel structural members. SEI/ASCE-8-02. Reston (VA); 2002.

[31] Australian/New Zealand Standard. Cold-formed stainless steel structures. AS/NZS 4673:2001. Sydney (Australia): Standards Australia; 2001.

[32] European Committee for Standardization. Eurocode 3: Design of steel structures – part 1-3: General rules – supplementary rules for cold formed members and sheeting. BS EN1993-1-3: 2006. Brussels: CEN; 2006.

[33] European Committee for Standardization. Eurocode 3: Design of steel structures – part 1-4: General rules – supplementary rules for stainless steels. BS EN1993-1-4: 2006. Brussels: CEN; 2006.

[34] Zhao X.L., Fernando D. and Al-Mahaidi R. CFRP strengthened RHS subjected to transverse end bearing force, Engineering Structures 2006; 28(11):1555-1565.

[35] AS 4100-1998 steel structures. Australian standard AS 4100-1998. Sydney, Australia: Standards Association of Australia; 1998.

[36] ABAQUS analysis user's manual, version 6.9-1. ABAQUS Inc., 2009.

[37] ASTM. Standard test methods for tension testing of metallic materials, E 8M-97. West Conshohocken: American Society for Testing and Materials; 1997.

[38] AS. Metallic materials – Tensile testing at ambient temperature. Australian Standard, AS 1391-2007. Sydney, Australia: Standards Association of Australia; 2007.

[39] AISI S100. North American Specification for the design of cold-formed steel structural members. North American Cold-formed Steel Specification, American Iron and Steel Institute, AISI S100-16, Washington, D.C., 2016..

[40] AS/NZS. Cold-formed steel structures, Australian/New Zealand standard AS/NZS 4600:2005. Sydney, Australia: Standards Australia; 2005.

[41] Huang Y. and Young B. Material properties of cold-formed lean duplex stainless steel sections, *Thin-Walled Structures*, 2012, 54: 72-81.

[42] Diehl T. Using ABAQUS cohesive elements to model peeling of an epoxy-bonded aluminum strip: A Benchmark study for inelastic peel arms, ABAQUS user conference, May 23-25, 2006, at The Charles Hotel, Cambridge, Massachusetts, USA.

[43] Campilho, R.D.S.G., de Moura, M.F.S.F. and Domingues, J.J.M.S. Using a cohesive damage model to predict the tensile behaviour of CFRP single-strap repairs. International Journal of Solids and Structures, 2008, 45(5), 1497-1512.

[44] ASCE. Minimum design loads for buildings and other structures, ASCE/SEI Standard 7-10. Virginia: American Society of Civil Engineers Standard; 2010.

[45] AISI S100. Commentary on North American Specification for the design of cold-formed steel structural members. Washington, DC: American Iron and Steel Institute; 2016.

[46] Zhou,F., and Young, B. Cold-formed stainless steel sections subjected to web crippling. Journal of Structural Engineering, 2006; ASCE, 132(1):134–144.

[47] Zhou, F., and Young, B. Experimental and numerical investigations of cold-formed stainless steel tubular sections subjected to concentrated bearing load." *Journal of Constructional Steel Research*, 2007, 63(11): 1452–1466.

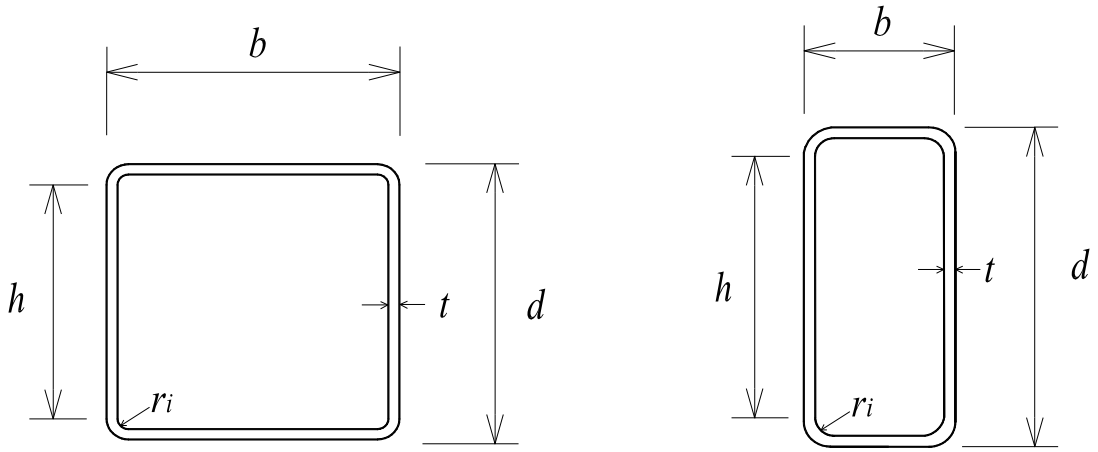

(a) Square hollow section (SHS) (b) Rectangular hollow section (RHS)

Figure 1: Designation of symbols of tubular stainless steel test specimens [20]

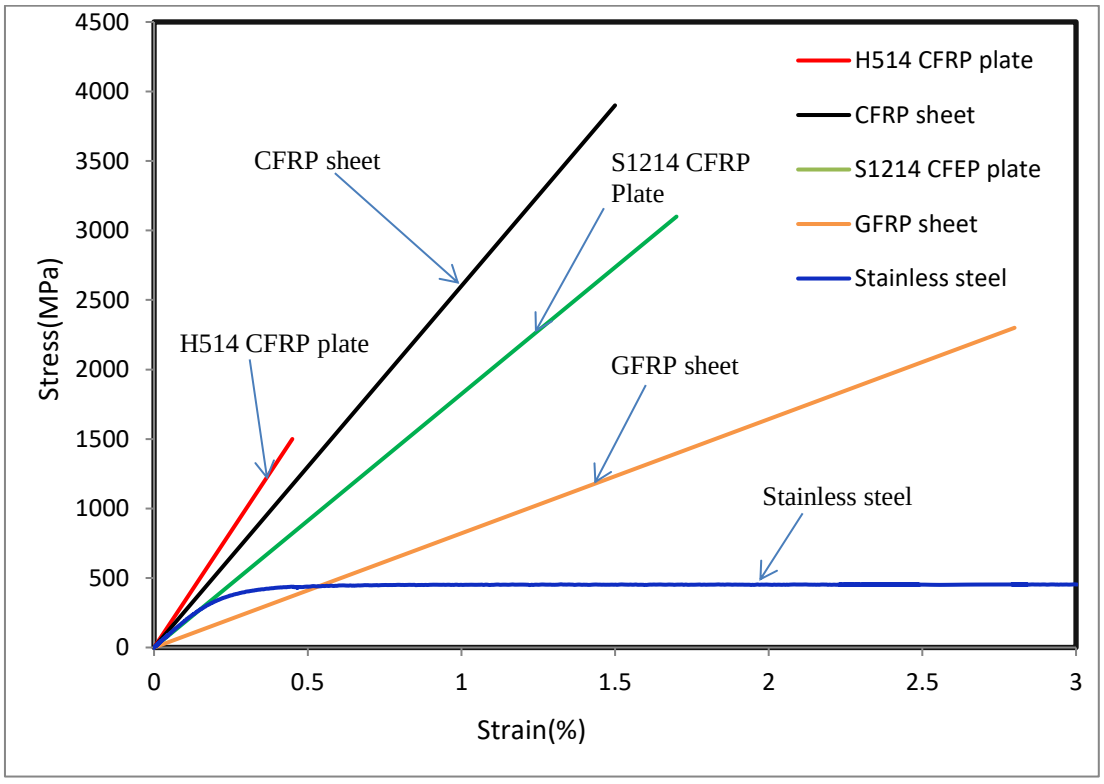

Figure 2: Representative stress-strain curves of stainless steel and FRP [24]

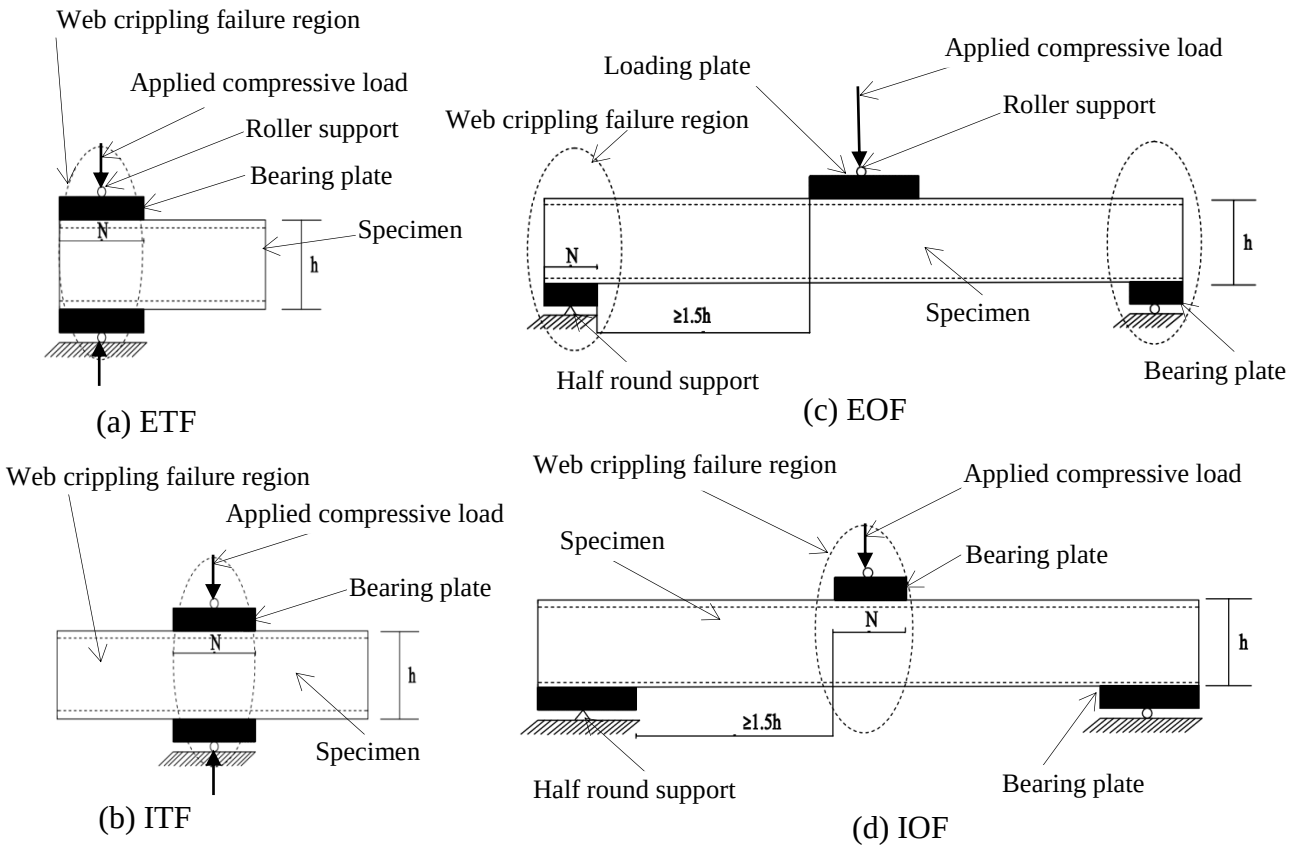

Figure 3: Four web crippling loading configurations

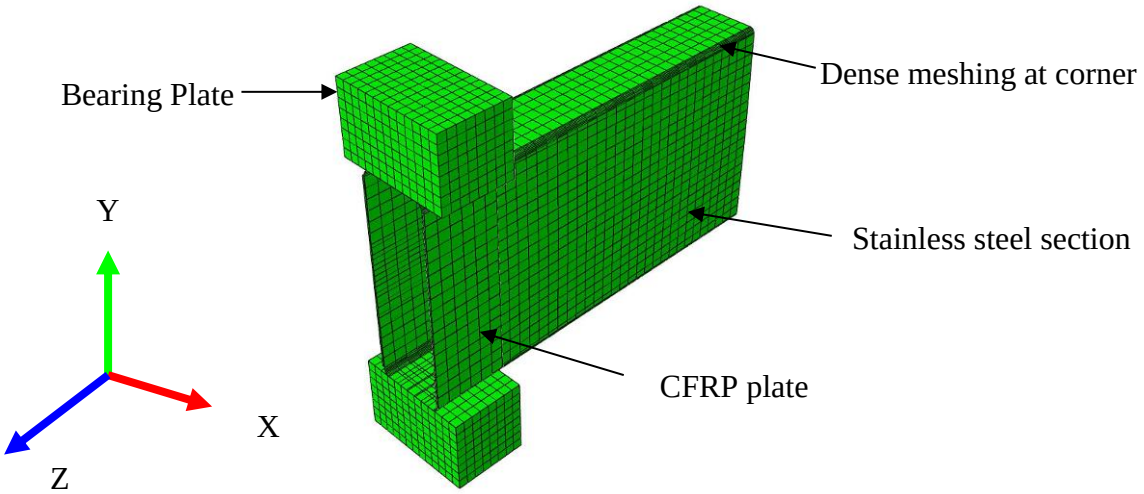

Figure 4: Details modeling and meshing of stainless steel section

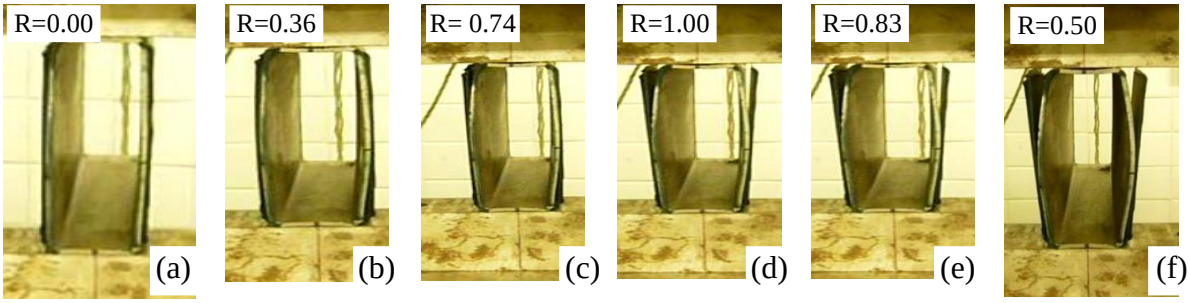

Figure 5: Experimental progressive damage mode of adhesive layer ((a) P = 0 kN, Δ = 0 mm, T = 0 Sec; (b) P = 9.73 kN, Δ = 0.19 mm, T = 38 Sec; (c) P = 19.95 kN, Δ = 0.38 mm, T = 76 Sec; (d) P = 26.8 kN, Δ = 1.12 mm, T = 224 Sec; (e) P = 22.37 kN, Δ = 1.78 mm, T = 356 Sec; (f) P = 13.32 kN, Δ = 4.3 mm, T = 860 Sec)

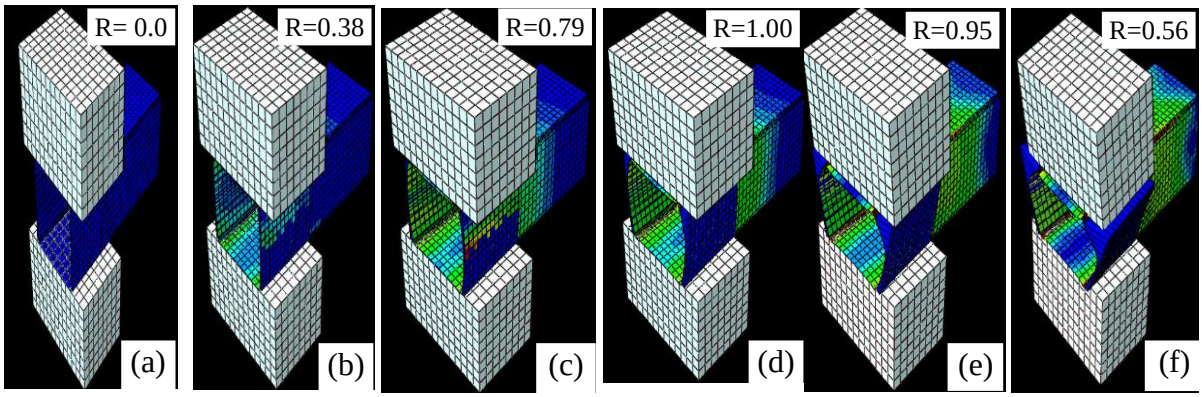

Figure 6: FEA progressive damage mode of adhesive layer ((a) P = 0 kN, Δ = 0 mm, T = 0 Sec; (b) P = 9.61 kN, Δ = 0.20 mm, T = 40 Sec; (c) P = 19.82 kN, Δ = 0.40 mm, T = 80 Sec; (d) P = 25.20 kN, Δ = 1.19 mm, T = 238 Sec; (e) P = 24.10 kN, Δ = 1.85 mm, T = 370 Sec; (f) P = 14.76 kN, Δ = 4.9 mm, T = 980 Sec)

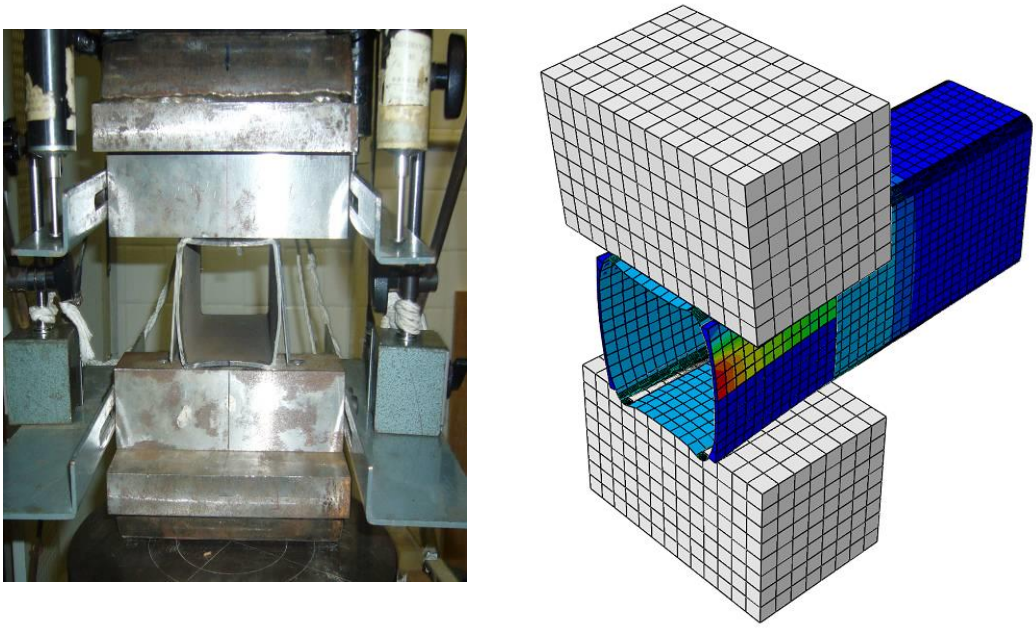

(a) Experimental [24] (b) FEA

Figure 7: Experimental and FEA debonding failure modes for Specimen F60×40×3-ETF-f1

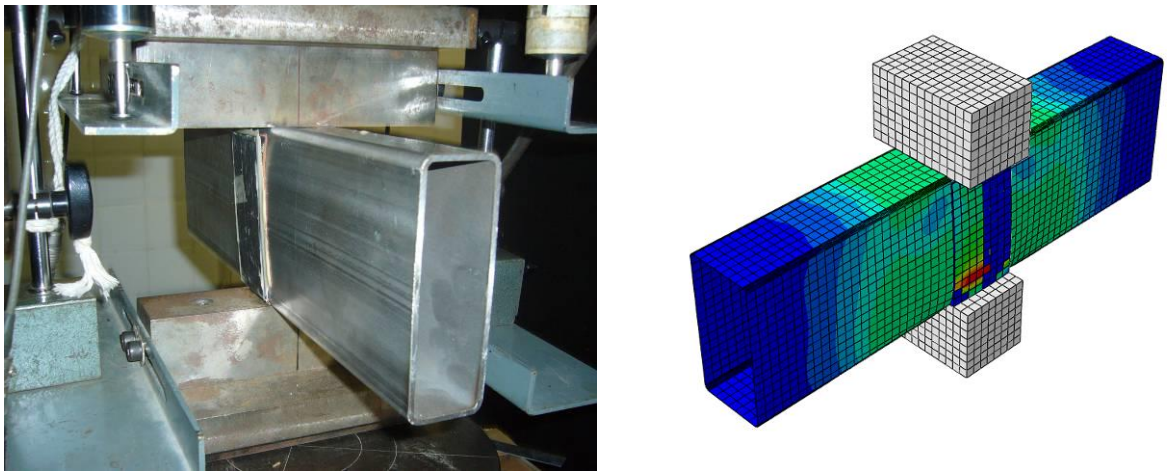

(a) Experimental [24] (b) FEA

Figure 8: Experimental and FEA failure modes for Specimen F120×40×3-ITF-f1

(a) Experimental [24]

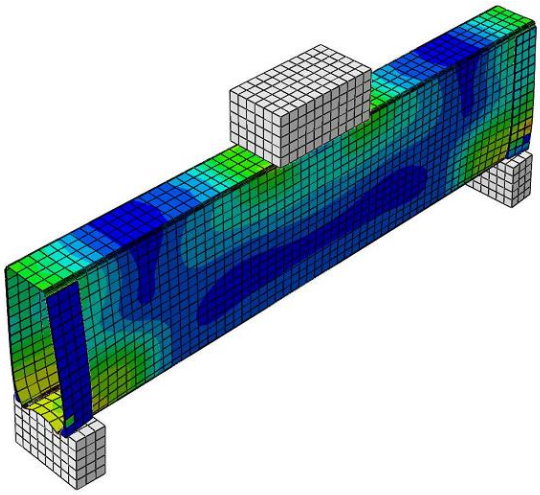

(b) FEA

Figure 9: Experimental and FEA failure modes for Specimen D150×50×2.5-EOF-d1

(a) Experimental [24]

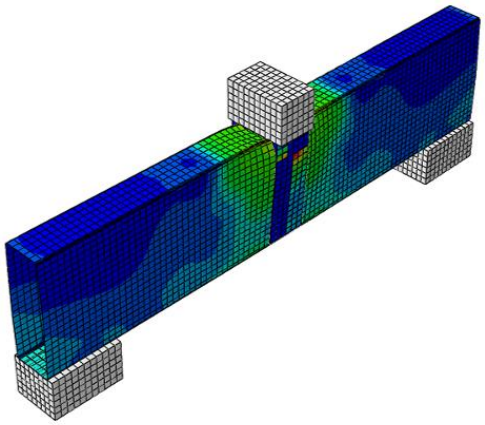

(b) FEA

Figure 10: Experimental and FEA failure modes for Specimen D150×50×2.5-IOF-d1

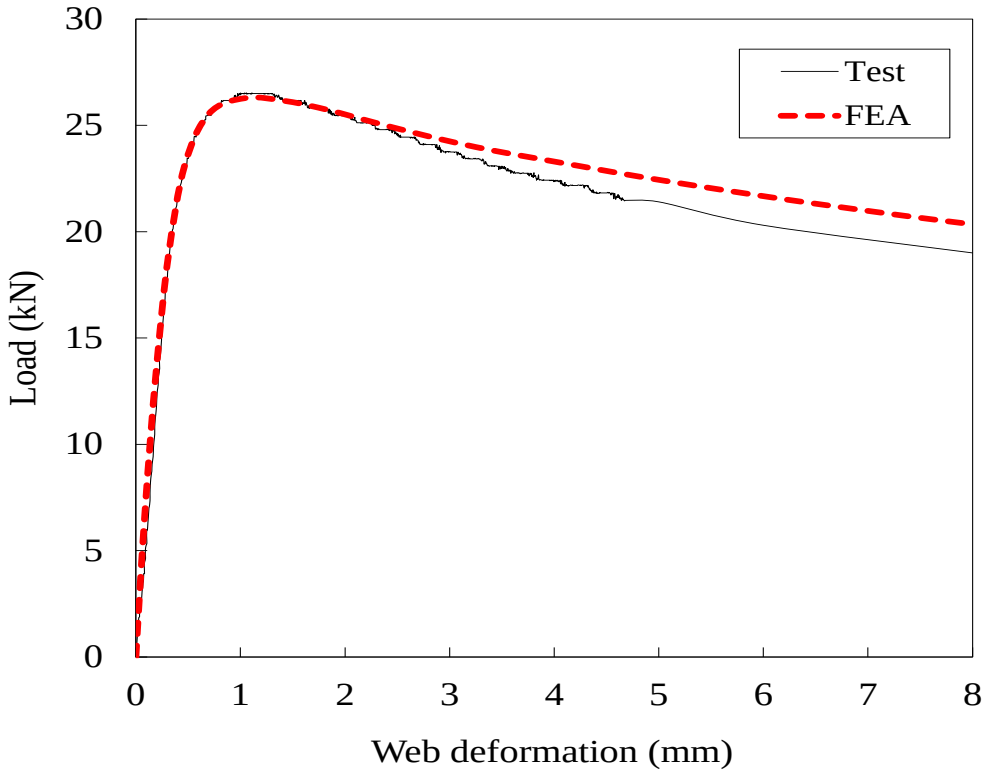

Figure 11: Comparison of load–web deformation from test [24] and FEA for Specimen D100×50×2.5-ETF-0

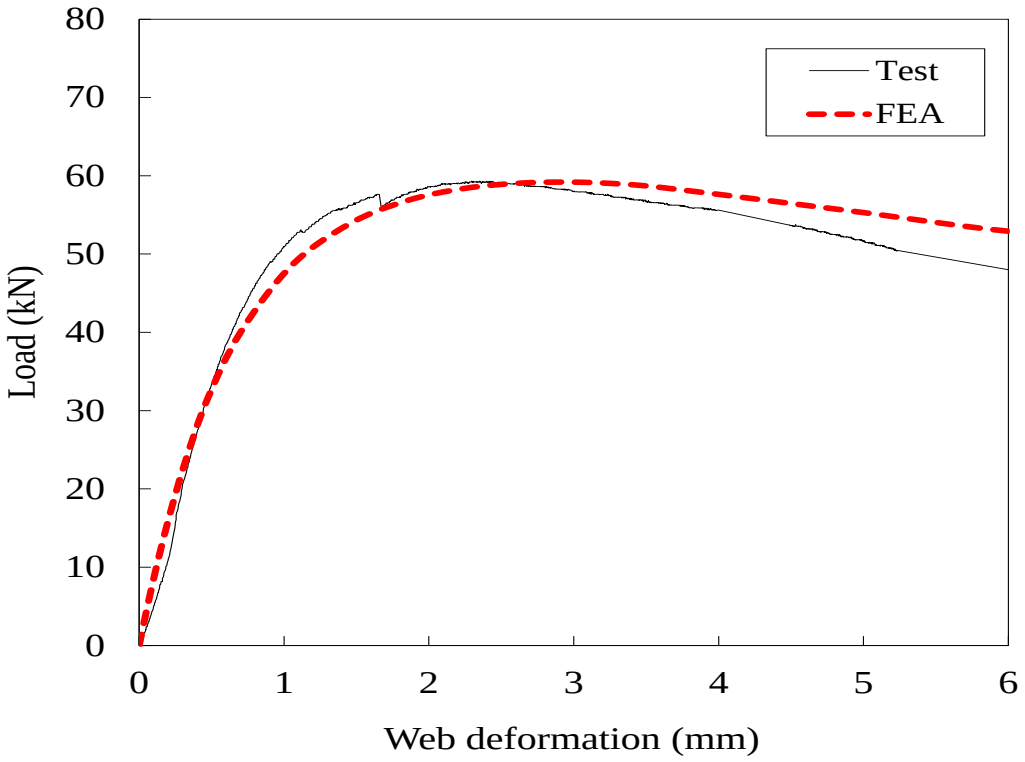

Figure 12: Comparison of load–web deformation from test [24] and FEA for Specimen D150×50×2.5-ITF-d1

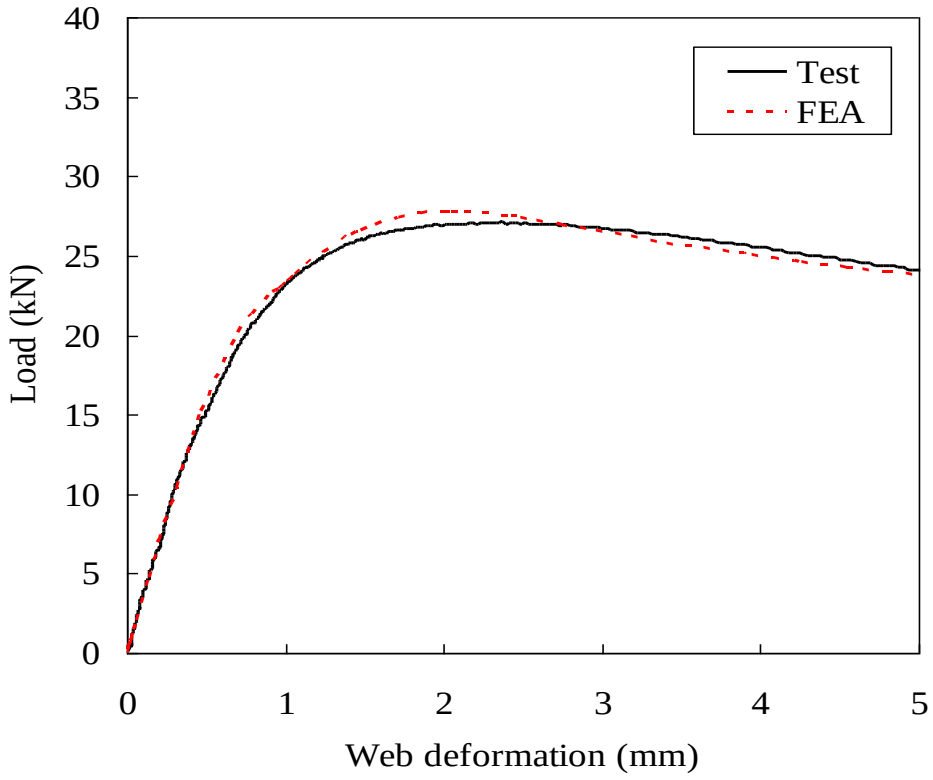

Figure 13: Comparison of load–web deformation from test [24] and FEA for Specimen F80×80×3-EOF-f1

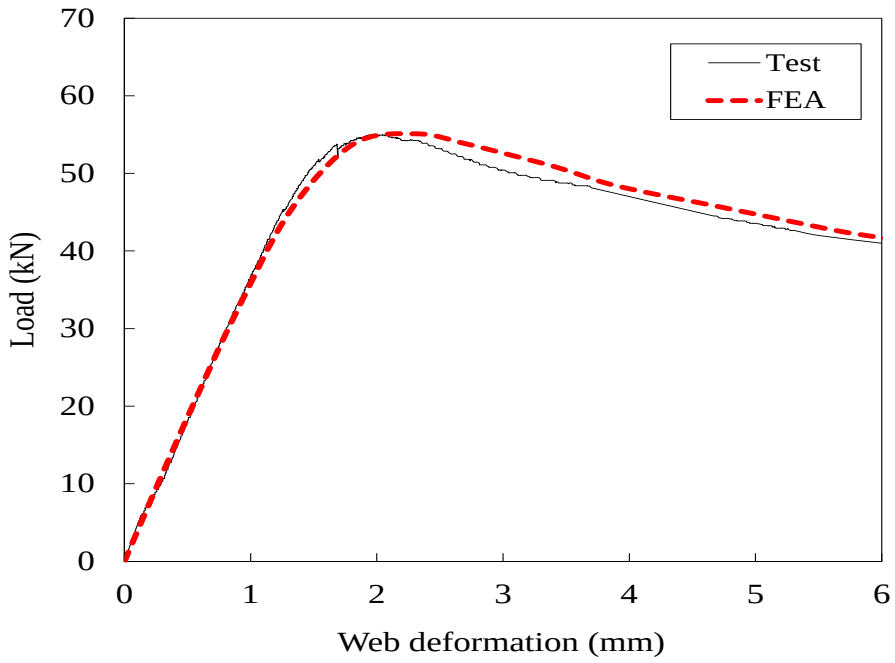

Figure 14: Comparison of load–web deformation from test [24] and FEA for Specimen D150×50×2.5-IOF-d1

Specimen	*h/t*	P_{Exp} (kN)	P_{FEA} (kN)	P_{Exp}/P_{FEA}
F50×50×4-ETF-0	8.9	39.5	40.8	0.97
F50×50×4-ETF-f1	9.0	43.8	43.1	1.02
F60×40×3-ETF-0	17.5	23.7	22.3	1.06
F60×40×3-ETF-f1	18.0	26.8	25.2	1.06
F80×80×3-ETF-0	24.1	23.0	22.4	1.03
F80×80×3-ETF-f1	24.6	26.9	27.2	0.99
F100×50×3-ETF-0	31.8	24.4	24.8	0.98
F100×50×3-ETF-f1	32.3	30.5	28.5	1.07
F120×40×3-ETF-0	37.4	20.7	20.1	1.03
F120×40×3-ETF-f1	37.7	31.2	28.5	1.09
Mean				1.03
COV				0.041

Table 1: Experimental versus FEA web crippling ultimate loads comparison under ETF loading condition for ferritic stainless steel [20]

Specimen	*h/t*	P_{Exp} (kN)	P_{FEA} (kN)	P_{Exp}/P_{FEA}
F50×50×4-ITF-0	9.1	76.2	76.5	1.00
F50×50×4-ITF-f1	9.1	77.8	79.4	0.98
F60×40×3-ITF-0	17.1	42.3	40.0	1.06
F60×40×3-ITF-f1	17.3	43.6	42.8	1.02
F80×80×3-ITF-0	24.0	48.2	46.2	1.04
F80×80×3-ITF-f1	24.2	49.5	50.4	0.98
F100×50×3-ITF-0	32.0	51.5	46.8	1.10
F100×50×3-ITF-f1	32.1	54.0	50.1	1.08
F120×40×3-ITF-0	37.7	45.5	45.1	1.01
F120×40×3-ITF-f1	38.2	49.8	48.2	1.03
Mean				1.03
COV				0.039

Table 2: Experimental versus FEA web crippling ultimate loads comparison under ITF loading condition for ferritic stainless steel [20]

Specimen	*h/t*	P_{Exp} (kN) Ref. [20]	P_{FEA} (kN)	P_{Exp}/P_{FEA}
F60×40×3-EOF-0	17.6	26.2	25.6	1.02
F60×40×3-EOF-f1(30)	17.9	26.6	27.5	0.97
F80×80×3-EOF-0	24.1	26.1	26.1	1.00
F80×80×3-EOF-f1(30)	24.7	27.1	27.8	0.98
F100×50×3-EOF-0	31.6	29.1	28.0	1.04
F100×50×3-EOF-f1(30)	31.7	31.3	31.4	1.00
F120×40×3-EOF-0	37.5	25.1	23.4	1.07
F120×40×3-EOF-f1(30)	37.7	27.9	25.8	1.08
Mean				1.02
COV				0.042

Table 3: Experimental [20] versus FEA web crippling ultimate loads comparison under EOF loading condition for ferritic stainless steel

Specimen	*h/t*	P_{Exp} (kN) Ref. [20]	P_{FEA} (kN)	P_{Exp}/P_{FEA}
F80×80×3-IOF-0	24.1	48.1	43.7	1.10
F80×80×3-IOF-f1	24.4	48.5	47.4	1.01
F100×50×3-IOF-0	31.8	44.2	41.4	1.07
F100×50×3-IOF-f1	31.9	45.4	44.5	1.02
F120×40×3-IOF-0	37.8	41.8	41.6	1.00
F120×40×3-IOF-f1	38.5	42.9	45.7	0.94
Mean				1.03
COV				0.054

Table 4: Experimental [20] versus FEA web crippling ultimate loads comparison under IOF loading condition for ferritic stainless steel

Specimen	*h/t*	P_{Exp} (kN) Ref. [21]	P_{FEA} (kN)	P_{Exp}/P_{FEA}
D50×50×1.5-EOF-0	29.4	13.2	12.4	1.06
D50×50×1.5-EOF-d1(30)	29.5	13.8	13.3	1.04
D100×50×2.5-EOF-0	36.7	37.3	35.2	1.06
D100×50×2.5-EOF-d1(30)	36.9	45.4	43.8	1.04
D150×50×2.5-EOF-0	56.5	25.6	24.4	1.05
D150×50×2.5-EOF-d1(30)	56.7	27.3	27.8	0.98
Mean				1.04
COV				0.029

Table 5: Experimental [21] versus FEA web crippling ultimate loads comparison under EOF loading condition for lean duplex stainless steel

Specimen	h/t	P_{Exp} (kN) Ref. [21]	P_{FEA} (kN)	P_{Exp}/P_{FEA}
D50×50×1.5-IOF-0	29.2	19.6	20.8	0.94
D50×50×1.5-IOF-d1	29.4	20.1	21.0	0.96
D100×50×2.5-IOF-0	36.8	60.5	60.7	1.00
D100×50×2.5-IOF-d1	36.8	62.8	65.8	0.96
D150×50×2.5-IOF-0	56.6	53.5	49.6	1.08
D150×50×2.5-IOF-d1	56.8	55.0	55.1	1.01
Mean				0.99
COV				0.051

Table 6: Experimental [21] versus FEA web crippling ultimate loads comparison under IOF loading for lean duplex stainless steel

Specimen	d	b	t	L	r_i	h/t	$P_{FEA,0}$ or P_{FEA}	$P_{FEA}/P_{FEA,0}$
	(mm)	(mm)	(mm)	(mm)	(mm)		(kN)	
F35×35×4-ETF-0	35	35	4.0	102.5	4.0	4.7	36.6	1.00
F35×35×4-ETF-f1	35	35	4.0	102.5	4.0	4.7	38.3	1.05
F60×60×2.5-ETF-0	60	60	2.5	140	2.5	20.0	17.6	1.00
F60×60×2.5-ETF-f1	60	60	2.5	140	2.5	20.0	20.6	1.17
F80×80×2-ETF-0	80	80	2.0	170	2.0	36.0	11.9	1.00
F80×80×2-ETF-f1	80	80	2.0	170	2.0	36.0	16.7	1.40
F100×50×1.7-ETF-0	100	50	1.7	200	1.7	54.8	8.6	1.00
F100×50×1.7-ETF-f1	100	50	1.7	200	1.7	54.8	13.1	1.52
F120×40×1.6-ETF-0	120	40	1.6	230	1.6	71.0	7.3	1.00
F120×40×1.6-ETF-f1	120	40	1.6	230	1.6	71.0	11.2	1.53
F150×50×1.6-ETF-0	150	50	1.6	275	1.6	89.7	6.9	1.00
F150×50×1.6-ETF-f1	150	50	1.6	275	1.6	89.7	9.9	1.43
F200×100×1.8-ETF-0	200	100	1.8	350	1.8	107.0	8.0	1.00
F200×100×1.8-ETF-f1	200	100	1.8	350	1.8	107.0	9.9	1.24

Table 7: FEA parametric section dimensions and comparison of web crippling strengths between ferritic stainless steel sections under ETF loading with and without CFRP-strengthening

Specimen	d	b	t	L	r_i	h/t	$P_{FEA,0}$ or P_{FEA}	$P_{FEA}/P_{FEA,0}$
	(mm)	(mm)	(mm)	(mm)	(mm)		(kN)	
F35×35×4-ITF-0	35	35	4.0	155	4.0	4.7	54.9	1.00
F35×35×4-ITF-f1	35	35	4.0	155	4.0	4.7	56.7	1.03
F60×60×2.5-ITF-0	60	60	2.5	230	2.5	20.0	30.6	1.00
F60×60×2.5-ITF-f1	60	60	2.5	230	2.5	20.0	32.4	1.06
F80×80×2-ITF-0	80	80	2.0	290	2.0	36.0	23.4	1.00
F80×80×2-ITF-f1	80	80	2.0	290	2.0	36.0	25.5	1.09
F100×50×1.7-ITF-0	100	50	1.7	350	1.7	54.8	17.9	1.00
F100×50×1.7-ITF-f1	100	50	1.7	350	1.7	54.8	20.9	1.17
F120×40×1.6-ITF-0	120	40	1.6	410	1.6	71.0	17.1	1.00
F120×40×1.6-ITF-f1	120	40	1.6	410	1.6	71.0	21.2	1.24
F150×50×1.6-ITF-0	150	50	1.6	500	1.6	89.7	16.4	1.00
F150×50×1.6-ITF-f1	150	50	1.6	500	1.6	89.7	21.1	1.28
F200×100×1.8-ITF-0	200	100	1.8	650	1.8	107.0	20.1	1.00
F200×100×1.8-ITF-f1	200	100	1.8	650	1.8	107.0	23.6	1.17

Table 8: FEA parametric section dimensions and comparison of web crippling strengths between ferritic stainless steel sections under ITF loading with and without CFRP-strengthening

Specimen	d	b	t	L	r_i	h/t	$P_{FEA,0}$ or P_{FEA}	$P_{FEA}/P_{FEA,0}$
	(mm)	(mm)	(mm)	(mm)	(mm)		(kN)	
F80×80×2-EOF-0	80	80	2.0	380	2.0	36.0	11.8	1.00
F80×80×2-EOF-f1(30)	80	80	2.0	380	2.0	36.0	12.7	1.08
F100×50×1.7-EOF-0	100	50	1.7	440	1.7	54.8	8.7	1.00
F100×50×1.7-EOF-f1(30)	100	50	1.7	440	1.7	54.8	10.7	1.23
F120×40×1.6-EOF-0	120	40	1.6	500	1.6	71.0	8.1	1.00
F120×40×1.6-EOF-f1(30)	120	40	1.6	500	1.6	71.0	11.4	1.41
F150×50×1.6-EOF-0	150	50	1.6	590	1.6	89.7	7.9	1.00
F150×50×1.6-EOF-f1(30)	150	50	1.6	590	1.6	89.7	11.5	1.46
F200×100×1.8-EOF-0	200	100	1.8	740	1.8	107.0	9.2	1.00
F200×100×1.8-EOF-f1(30)	200	100	1.8	740	1.8	107.0	11.6	1.26

Table 9: FEA parametric section dimensions and comparison of web crippling strengths between ferritic stainless steel sections under EOF loading with and without CFRP-strengthening

Specimen	d	b	t	L	r_i	h/t	$P_{FEA,0}$ or P_{FEA}	$P_{FEA}/P_{FEA,0}$
	(mm)	(mm)	(mm)	(mm)	(mm)		(kN)	
F80×80×2-IOF-0	80	80	2.0	470	2.0	36.0	21.1	1.00
F80×80×2-IOF-f1	80	80	2.0	470	2.0	36.0	23.1	1.09
F100×50×1.7-IOF-0	100	50	1.7	530	1.7	54.8	15.6	1.00
F100×50×1.7-IOF-f1	100	50	1.7	530	1.7	54.8	18.9	1.21
F120×40×1.6-IOF-0	120	40	1.6	590	1.6	71.0	14.5	1.00
F120×40×1.6-IOF-f1	120	40	1.6	590	1.6	71.0	18.6	1.28
F150×50×1.6-IOF-0	150	50	1.6	680	1.6	89.7	15.6	1.00
F150×50×1.6-IOF-f1	150	50	1.6	680	1.6	89.7	19.6	1.26
F200×100×1.8-IOF-0	200	100	1.8	830	1.8	107.0	19.0	1.00
F200×100×1.8-IOF-f1	200	100	1.8	830	1.8	107.0	22.7	1.19

Table 10: FEA parametric section dimensions and comparison of web crippling strengths between ferritic stainless steel sections under IOF loading with and without CFRP-strengthening

Specimen	d	b	t	L	r_i	h/t	$P_{FEA,0}$ or P_{FEA}	$P_{FEA}/P_{FEA,0}$
	(mm)	(mm)	(mm)	(mm)	(mm)		(kN)	
D50×40×4.5-ETF-0	50	40	4.5	125	4.5	7.1	60.2	1.00
D50×40×4.5-ETF-f1	50	40	4.5	125	4.5	7.1	62.6	1.04
D70×70×3-ETF-0	70	70	3.0	155	3.0	19.3	29.2	1.00
D70×70×3-ETF-f1	70	70	3.0	155	3.0	19.3	32.2	1.10
D80×40×2-ETF-0	80	40	2.0	170	2.0	36.0	14.6	1.00
D80×40×2-ETF-f1	80	40	2.0	170	2.0	36.0	18.7	1.28
D100×100×1.8-ETF-0	100	100	1.8	200	1.8	51.6	11.4	1.00
D100×100×1.8-ETF-f1	100	100	1.8	200	1.8	51.6	16.7	1.46
D120×40×1.7-ETF-0	120	40	1.7	230	1.7	66.6	9.6	1.00
D120×40×1.7-ETF-f1	120	40	1.7	230	1.7	66.6	14.1	1.47
D150×150×1.8-ETF-0	150	150	1.8	275	1.8	79.3	10.6	1.00
D150×150×1.8-ETF-f1	150	150	1.8	275	1.8	79.3	13.7	1.29
D200×100×2-ETF-0	200	100	2.0	350	2.0	96.0	11.7	1.00
D200×100×2-ETF-f1	200	100	2.0	350	2.0	96.0	13.8	1.18
D200×50×1.7-ETF-0	200	50	1.7	350	1.7	113.6	8.2	1.00
D200×50×1.7-ETF-f1	200	50	1.7	350	1.7	113.6	10.4	1.26

Table 11: FEA parametric section dimensions and comparison of web crippling strengths between lean duplex stainless steel sections under ETF loading with and without CFRP-strengthening

Specimen	d	b	t	L	r_i	h/t	$P_{FEA,0}$ or P_{FEA}	$P_{FEA}/P_{FEA,0}$
	(mm)	(mm)	(mm)	(mm)	(mm)		(kN)	
D50×40×4.5-ITF-0	50	40	4.5	200	4.5	7.1	95.5	1.00
D50×40×4.5-ITF-f1	50	40	4.5	200	4.5	7.1	97.6	1.02
D70×70×3-ITF-0	70	70	3.0	260	3.0	19.3	55.6	1.00
D70×70×3-ITF-f1	70	70	3.0	260	3.0	19.3	59.0	1.06
D80×40×2-ITF-0	80	40	2.0	290	2.0	36.0	30.8	1.00
D80×40×2-ITF-f1	80	40	2.0	290	2.0	36.0	34.2	1.11
D100×100×1.8-ITF-0	100	100	1.8	350	1.8	51.6	28.4	1.00
D100×100×1.8-ITF-f1	100	100	1.8	350	1.8	51.6	33.1	1.16
D120×40×1.7-ITF-0	120	40	1.7	410	1.7	66.6	25.2	1.00
D120×40×1.7-ITF-f1	120	40	1.7	410	1.7	66.6	30.1	1.19
D150×150×1.8-ITF-0	150	150	1.8	500	1.8	79.3	31.0	1.00
D150×150×1.8-ITF-f1	150	150	1.8	500	1.8	79.3	34.4	1.11
D200×100×2-ITF-0	200	100	2.0	650	2.0	96.0	32.8	1.00
D200×100×2-ITF-f1	200	100	2.0	650	2.0	96.0	37.7	1.15
D200×50×1.7-ITF-0	200	50	1.7	650	1.7	113.6	24.7	1.00
D200×50×1.7-ITF-f1	200	50	1.7	650	1.7	113.6	29.4	1.19

Table 12: FEA parametric section dimensions and comparison of web crippling strengths between lean duplex stainless sections under ITF loading with and without CFRP-strengthening

Specimen	d	b	t	L	r_i	h/t	$P_{FEA,0}$ or P_{FEA}	$P_{FEA}/P_{FEA,0}$
	(mm)	(mm)	(mm)	(mm)	(mm)		(kN)	
D80×40×2-EOF-0	80	40	2.0	380	2.0	36.0	16.1	1.00
D80×40×2-EOF-f1(30)	80	40	2.0	380	2.0	36.0	18.3	1.14
D100×100×1.8-EOF-0	100	100	1.8	440	1.8	51.6	14.0	1.00
D100×100×1.8-EOF-f1(30)	100	100	1.8	440	1.8	51.6	18.5	1.32
D120×40×1.7-EOF-0	120	40	1.7	500	1.7	66.6	12.0	1.00
D120×40×1.7-EOF-f1(30)	120	40	1.7	500	1.7	66.6	15.7	1.31
D150×150×1.8-EOF-0	150	150	1.8	590	1.8	79.3	14.1	1.00
D150×150×1.8-EOF-f1(30)	150	150	1.8	590	1.8	79.3	18.1	1.28
D200×100×2-EOF-0	200	100	2.0	740	2.0	96.0	15.3	1.00
D200×100×2-EOF-f1(30)	200	100	2.0	740	2.0	96.0	18.3	1.20
D200×50×1.7-EOF-0	200	50	1.7	740	1.7	113.6	11.5	1.00
D200×50×1.7-EOF-f1(30)	200	50	1.7	740	1.7	113.6	14.0	1.22

Table 13: FEA parametric section dimensions and comparison of web crippling strengths between lean duplex stainless sections under EOF loading with and without CFRP-strengthening

Specimen	d	b	t	L	r_i	h/t	$P_{FEA,0}$ or P_{FEA}	$P_{FEA}/P_{FEA,0}$
	(mm)	(mm)	(mm)	(mm)	(mm)		*(kN)*	
D80×40×2-IOF-0	80	40	2.0	470	2.0	36.0	27.7	1.00
D80×402-IOF-f1	80	40	2.0	470	2.0	36.0	30.5	1.10
D100×100×1.8-IOF-0	100	100	1.8	530	1.8	51.6	26.7	1.00
D100×100×1.8-IOF-f1	100	100	1.8	530	1.8	51.6	31.5	1.18
D120×40×1.7-IOF-0	120	40	1.7	590	1.7	66.6	22.4	1.00
D120×40×1.7-IOF-f1	120	40	1.7	590	1.7	66.6	26.7	1.19
D150×150×1.8-IOF-0	150	150	1.8	680	1.8	79.3	29.3	1.00
D150×150×1.8-IOF-f1	150	150	1.8	680	1.8	79.3	33.9	1.16
D200×100×2-IOF-0	200	100	2.0	830	2.0	96.0	30.8	1.00
D200×100×2-IOF-f1	200	100	2.0	830	2.0	96.0	34.9	1.13
D200×50×1.7-IOF-0	200	50	1.7	830	1.7	113.6	23.5	1.00
D200×50×1.7-IOF-f1	200	50	1.7	830	1.7	113.6	27.8	1.18

Table 14: FEA parametric section dimensions and comparison of web crippling strengths between lean duplex stainless sections under IOF loading with and without CFRP-strengthening

Specimen	$f_{0.2}$ (MPa)	h/t	r_i/t	N/t	N/h	$A_{bonding}$ (mm)	P_{Exp} or P_{FEA} (kN)	$\frac{P_{Exp} \text{ or } P_{FEA}}{P_p}$
F35×35×4-ETF-0	434	4.7	1.0	12.5	2.6	0	36.6	0.90
F35×35×4-ETF-f1	434	4.7	1.0	12.5	2.6	950	38.3	0.93
F50×50×4-ETF-0	504	8.9	1.0	12.9	1.5	0	39.5	0.91
F50×50×4-ETF-f1	504	9.0	1.0	13.0	1.5	1721	43.8	1.00
F50×50×4-ETF-f1-R	504	9.1	1.1	13.2	1.4	1725	43.3	1.01
F60×40×3-ETF-0	430	17.5	1.1	18.0	1.0	0	23.7	1.15
F60×40×3-ETF-f1	430	18.0	1.1	18.5	1.0	2430	26.8	1.29
F60×60×2.5-ETF-0	434	20.0	1.0	20.0	1.0	0	17.6	1.00
F60×60×2.5-ETF-f1	434	20.0	1.0	20.0	1.0	2500	20.6	1.09
F80×80×3-ETF-0	434	24.1	1.2	17.8	0.7	0	23.0	1.12
F80×80×3-ETF-f1	434	24.6	1.2	18.1	0.7	3398	26.9	1.25
F100×50×3-ETF-0	472	31.8	1.0	17.8	0.6	0	24.4	1.07
F100×50×3-ETF-f1	472	32.3	1.0	18.1	0.6	4454	30.5	1.26
F80×80×2-ETF-0	434	36.0	1.0	25.0	0.7	0	11.9	1.01
F80×80×2-ETF-f1	434	36.0	1.0	25.0	0.7	3600	16.7	1.23
F120×40×3-ETF-0	426	37.4	1.4	17.6	0.47	0	20.7	1.10
F120×40×3-ETF-f1	426	37.7	1.4	17.7	0.47	5313	31.2	1.47
F100×50×1.7-ETF-0	434	54.8	1.0	29.4	0.5	0	8.6	0.98
F100×50×1.7-ETF-f1	434	54.8	1.0	29.4	0.5	4660	13.1	1.18
F120×40×1.6-ETF-0	434	71.0	1.0	31.3	0.4	0	7.3	0.94
F120×40×1.6-ETF-f1	434	71.0	1.0	31.3	0.4	5680	11.2	1.06
F150×50×1.6-ETF-0	434	89.8	1.0	31.3	0.3	0	6.9	0.91
F150×50×1.6-ETF-f1	434	89.8	1.0	31.3	0.3	7180	9.9	0.89
F200×100×1.8-ETF-0	434	107.0	1.0	27.8	0.3	0	8.0	0.89
F200×100×1.8-ETF-f1	434	107.0	1.0	27.8	0.3	9640	9.9	0.72
Mean, P_m								1.05
COV, V_p								0.155
Reliability index, ß								2.52
Resistance factor, ϕ_w								0.85

Table 15: Web crippling test strengths verses predicted design strengths for ferritic stainless steel specimens under ETF loading

Specimen	$f_{0.2}$ (MPa)	h/t	r_i/t	N/t	N/h	$A_{bonding}$ (mm)	P_{Exp} or P_{FEA} (kN)	$\frac{P_{Exp} \text{ or } P_{FEA}}{P_p}$
F35×35×4-ITF-0	434	4.7	1.0	12.5	2.6	0	54.9	0.74
F35×35×4-ITF-f1	434	4.7	1.0	12.5	2.6	950	56.7	0.75
F50×50×4-ITF-0	504	9.1	1.1	13.2	1.5	0	76.2	0.97
F50×50×4-ITF-f1	504	9.1	1.1	13.2	1.4	1727	77.8	0.98
F50×50×4-ITF-f1-R	504	9.2	1.1	13.2	1.4	1728	77.6	0.98
F60×40×3-ITF-0	430	17.1	1.1	17.7	1.0	0	42.3	1.04
F60×60×3-ITF-f1	430	17.3	1.1	17.8	1.0	2420	43.6	1.04
F60×60×2.5-ITF-0	434	20.0	1.0	20.0	1.0	0	30.6	0.90
F60×60×2.5-ITF-f1	434	20.0	1.0	20.0	1.0	2500	32.4	0.90
F80×80×3-ITF-0	434	24.0	1.2	17.7	0.7	0	48.2	1.19
F80×80×3-ITF-f1	434	24.2	1.2	17.8	0.7	3399	49.5	1.16
F100×50×3-ITF-0	472	32.0	1.0	17.9	0.6	0	51.5	1.16
F100×50×3-ITF-f1	472	32.1	1.0	18.0	0.6	4457	54.0	1.14
F80×80×2-ITF-0	434	36.0	1.0	25.0	0.7	0	23.4	1.00
F80×80×2-ITF-f1	434	36.0	1.0	25.0	0.7	3600	25.5	0.97
F120×40×3-ITF-0	426	37.7	1.4	17.8	0.47	0	45.5	1.20
F120×40×3-ITF-f1	426	38.2	1.4	17.9	0.47	5321	49.8	1.21
F100×50×1.7-ITF-0	434	54.8	1.0	29.4	0.5	0	17.9	1.00
F100×50×1.7-ITF-f1	434	54.8	1.0	29.4	0.5	4660	20.9	0.97
F120×40×1.6-ITF-0	434	71.0	1.0	31.3	0.4	0	17.1	1.05
F120×40×1.6-ITF-f1	434	71.0	1.0	31.3	0.4	5680	21.2	1.02
F150×50×1.6-ITF-0	434	89.7	1.0	31.3	0.3	0	16.4	1.01
F150×50×1.6-ITF-f1	434	89.7	1.0	31.3	0.3	7180	21.1	0.97
F200×100×1.8-ITF-0	434	107.1	1.0	27.8	0.3	0	20.1	1.02
F200×100×1.8-ITF-f1	434	107.1	1.0	27.8	0.3	9640	23.6	0.87
Mean, P_m								1.01
COV, V_p								0.123
Reliability index, ß								2.53
Resistance factor, ϕ_w								0.85

Table 16: Web crippling test strengths verses predicted design strengths for ferritic stainless steel specimens under ITF loading

Specimen	$f_{0.2}$ (MPa)	h/t	r_i/t	N/t	N/h	$A_{bonding}$ (mm)	P_{Exp} or P_{FEA} (kN)	$\frac{P_{Exp} \text{ or } P_{FEA}}{P_p}$
F60×40×3-EOF-0	430	17.6	1.1	10.9	0.6	0	26.2	1.12
F60×40×3-EOF-f1(30)	430	17.9	1.1	11.0	0.6	1457	26.6	1.11
F80×80×3-EOF-0	434	24.1	1.2	10.7	0.4	0	26.1	1.09
F80×80×3-EOF-f1(30)	434	24.7	1.2	10.9	0.4	2040	27.1	1.10
F100×50×3-EOF-0	472	31.6	1.0	10.7	0.3	0	29.1	1.12
F100×50×3-EOF-f1(30)	472	31.7	1.0	10.7	0.3	2670	31.3	1.12
F80×80×2-EOF-0	434	36.0	1.0	15.0	0.4	0	11.8	0.89
F80×80×2-EOF-f1(30)	434	36.0	1.0	15.0	0.4	2160	12.7	0.85
F120×40×3-EOF-0	426	37.5	1.4	10.6	0.3	0	25.1	1.10
F120×40×3-EOF-f1(30)	426	37.7	1.4	10.6	0.3	3194	27.9	1.11
F100×50×1.7-EOF-0	434	54.8	1.0	17.6	0.3	0	8.7	0.89
F100×50×1.7-EOF-f1(30)	434	54.8	1.0	17.6	0.3	2796	10.7	0.89
F120×40×1.6-EOF-0	434	71.0	1.0	18.8	0.3	0	8.1	0.94
F120×40×1.6-EOF-f1(30)	434	71.0	1.0	18.8	0.3	3408	11.4	1.01
F150×50×1.6-EOF-0	434	89.7	1.0	18.8	0.2	0	7.9	0.94
F150×50×1.6-EOF-f1(30)	434	89.7	1.0	18.8	0.2	4308	11.5	0.97
F200×100×1.8-EOF-0	434	107.0	1.0	16.7	0.2	0	9.2	0.92
F200×100×1.8-EOF-f1(30)	434	107.0	1.0	16.7	0.2	5784	11.6	0.80
Mean, P_m								1.00
COV, V_p								0.111
Reliability index, ß								2.53
Resistance factor, ϕ_w								0.85

Table 17: Web crippling test strengths verses predicted design strengths for ferritic stainless steel specimens under EOF loading

Specimen	$f_{0.2}$ (MPa)	h/t	r_i/t	N/t	N/h	$A_{bonding}$ (mm)	P_{Exp} or P_{FEA} (kN)	$\frac{P_{Exp} \text{ or } P_{FEA}}{P_p}$
F80×80×3-IOF-0	434	24.1	1.2	17.8	0.7	0	48.1	1.14
F80×80×3-IOF-f1	434	24.4	1.2	18.0	0.7	3397	48.5	1.13
F100×50×3-IOF-0	472	31.8	1.0	17.9	0.6	0	44.2	0.96
F100×50×3-IOF-f1	472	31.9	1.0	17.9	0.6	4451	45.4	0.94
F100×50×3-IOF-f1-R	472	31.9	1.0	17.9	0.6	4456	45.6	0.95
F80×80×2-IOF-0	434	36.0	1.0	25.0	0.7	0	21.1	0.91
F80×80×2-IOF-f1	434	36.0	1.0	25.0	0.7	3600	23.1	0.92
F120×40×3-IOF-0	426	37.8	1.4	17.8	0.5	0	41.8	1.06
F120×40×3-IOF-f1	426	38.5	1.4	18.1	0.5	5328	42.9	1.05
F100×50×1.7-IOF-0	434	54.8	1.0	29.4	0.5	0	15.6	0.91
F100×50×1.7-IOF-f1	434	54.8	1.0	29.4	0.5	4660	18.9	0.97
F120×40×1.6-IOF-0	434	71.0	1.0	31.3	0.4	0	14.5	0.95
F120×40×1.6-IOF-f1	434	71.0	1.0	31.3	0.4	5680	18.6	1.03
F150×50×1.6-IOF-0	434	89.7	1.0	31.3	0.3	0	15.6	1.03
F150×50×1.6-IOF-f1	434	89.7	1.0	31.3	0.3	7180	19.6	1.05
F200×100×1.8-IOF-0	434	107.0	1.0	27.8	0.3	0	19.0	1.03
F200×100×1.8-IOF-f1	434	107.0	1.0	27.8	0.3	9640	22.7	0.98
Mean, P_m								1.00
COV, V_p								0.072
Reliability index, ß								2.71
Resistance factor, ϕ_w								0.85

Table 18: Web crippling test strengths verses predicted design strengths for ferritic stainless steel specimens under IOF loading

Specimen	$f_{0.2}$ (MPa)	h/t	r_i/t	N/t	N/h	$A_{bonding}$ (mm)	P_{Exp} or P_{FEA} (kN)	$\frac{P_{Exp} \text{ or } P_{FEA}}{P_p}$
D50×40×4.5-ETF-0	606	7.1	1.0	11.1	1.6	0	60.2	0.87
D50×40×4.5-ETF-d1	606	7.1	1.0	11.1	1.6	1600	62.6	0.89
D30×50×2.5-ETF-0	774	8.2	0.8	19.5	2.4	0	41.8	1.15
D30×50×2.5-ETF-d1	774	8.2	0.8	19.6	2.4	1045	43.6	1.20
D50×50×2.5-ETF-0	663	17.1	0.4	19.9	1.2	0	41.3	1.31
D50×50×2.5-ETF-d1	663	17.0	0.4	20.0	1.2	2125	42.8	1.32
D70×70×3-ETF-0	606	19.3	1.0	16.7	0.9	0	29.2	0.90
D70×70×3-ETF-d1	606	19.3	1.0	16.7	0.9	2900	32.2	0.95
D50×50×1.5-ETF-0	595	29.3	0.6	32.4	1.1	0	11.4	1.03
D50×50×1.5-ETF-d1	595	29.7	0.7	32.8	1.1	2267	12.8	1.07
D50×50×1.5-ETF-d1-R	595	29.7	0.7	32.7	1.1	2277	12.9	1.07
D100×50×2.5-ETF-0	606	36.6	0.5	19.8	0.5	0	26.5	1.03
D100×50×2.5-ETF-d1	606	36.9	0.5	19.9	0.5	4634	45.5	1.65
D80×40×2-ETF-0	606	36.0	1.0	25.0	0.7	0	14.6	0.95
D80×40×2-ETF-d1	606	36.0	1.0	25.0	0.7	3600	18.7	1.09
D150×50×2.5-ETF-0	620	55.9	1.0	20.0	0.4	0	19.9	0.95
D150×50×2.5-ETF-d1	620	56.2	1.0	20.1	0.4	6991	24.2	1.00
D100×100×1.8-ETF-0	606	51.6	1.0	27.8	0.5	0	11.4	0.94
D100×100×1.8-ETF-d1	606	51.6	1.0	27.8	0.5	4640	16.7	1.16
D120×40×1.7-ETF-0	606	66.6	1.0	29.4	0.4	0	9.6	0.92
D120×40×1.7-ETF-d1	606	66.6	1.0	29.4	0.4	5660	14.1	1.07
D150×150×1.8-ETF-0	606	79.3	1.0	27.8	0.4	0	10.6	0.97
D150×150×1.8-ETF-d1	606	79.3	1.0	27.8	0.4	7140	13.7	0.95
D200×100×2-ETF-0	606	96.0	1.0	25.0	0.3	0	11.7	0.95
D200×100×2-ETF-d1	606	96.0	1.0	25.0	0.3	9600	13.8	0.81
D200×50×1.7-ETF-0	606	113.6	1.0	29.4	0.3	0	8.2	0.92
D200×50×1.7-ETF-d1	606	113.6	1.0	29.4	0.3	9660	10.4	0.77
Mean, P_m								1.03
COV, V_p								0.176
Reliability index, ß								2.55
Resistance factor, ϕ_w								0.80

Table 19: Web crippling test strengths verses predicted design strengths for lean duplex stainless steel specimens under ETF loading

Specimen	$f_{0.2}$ (MPa)	h/t	r_i/t	N/t	N/h	$A_{bonding}$ (mm)	P_{Exp} or P_{FEA} (kN)	$\frac{P_{Exp} \text{ or } P_{FEA}}{P_p}$
D50×40×4.5-ITF-0	606	7.1	1.0	11.1	1.6	0	95.5	0.73
D50×40×4.5-ITF-d1	606	7.1	1.0	11.1	1.6	1600	97.6	0.74
D30×50×2.5-ITF-0	774	8.1	0.8	19.3	2.4	0	66.9	0.96
D30×50×2.5-ITF-d1	774	8.1	0.8	19.4	2.4	1042	67.3	0.97
D50×50×2.5-ITF-0	663	17.2	0.4	19.9	1.2	0	67.2	1.12
D50×50×2.5-ITF-d1	663	17.0	0.4	19.9	1.2	2134	68.5	1.11
D70×70×3-ITF-0	606	19.3	1.0	16.7	0.9	0	55.6	0.85
D70×70×3-ITF-d1	606	19.3	1.0	16.7	0.9	2900	59.0	0.87
D50×50×1.5-ITF-0	595	29.2	0.6	32.4	1.1	0	22.6	0.99
D50×50×1.5-ITF-d1	595	29.1	0.6	32.4	1.1	2246	23.6	0.97
D100×50×2.5-ITF-0	606	36.8	0.5	19.9	0.5	0	69.2	1.31
D100×50×2.5-ITF-d1	606	36.9	0.5	19.9	0.5	4634	71.5	1.27
D100×50×2.5-ITF-d1-R	606	36.8	0.5	19.9	0.5	4624	72.1	1.28
D80×40×2-ITF-0	606	36.0	1.0	25.0	0.7	0	30.8	0.94
D80×40×2-ITF-d1	606	36.0	1.0	25.0	0.7	3600	34.2	0.96
D150×50×2.5-ITF-0	620	56.7	1.0	20.3	0.4	0	58.6	1.25
D150×50×2.5-ITF-d1	620	57.0	1.0	20.3	0.4	6999	59.3	1.15
D100×100×1.8-ITF-0	606	51.6	1.0	27.8	0.5	0	28.4	1.04
D100×100×1.8-ITF-d1	606	51.6	1.0	27.8	0.5	4640	33.1	1.08
D120×40×1.7-ITF-0	606	66.6	1.0	29.4	0.4	0	25.2	1.02
D120×40×1.7-ITF-d1	606	66.6	1.0	29.4	0.4	5660	30.1	1.05
D150×150×1.8-ITF-0	606	79.3	1.0	27.8	0.4	0	31.0	1.15
D150×150×1.8-ITF-d1	606	79.3	1.0	27.8	0.4	7140	34.4	1.07
D200×100×2-ITF-0	606	96.0	1.0	25.0	0.3	0	32.8	1.04
D200×100×2-ITF-d1	606	96.0	1.0	25.0	0.3	9600	37.7	0.98
D200×50×1.7-ITF-0	606	113.6	1.0	29.4	0.3	0	24.7	1.03
D200×50×1.7-ITF-d1	606	113.6	1.0	29.4	0.3	9660	29.4	0.95
Mean, P_m								1.03
COV, V_p								0.143
Reliability index, ß								2.52
Resistance factor, ϕ_w								0.85

Table 20: Web crippling test strengths verses predicted design strengths for lean duplex stainless steel specimens under ITF loading

Specimen	$f_{0.2}$ (MPa)	h/t	r_i/t	N/t	N/h	$A_{bonding}$ (mm)	P_{Exp} or P_{FEA} (kN)	$\frac{P_{Exp} \text{ or } P_{FEA}}{P_p}$
D50×50×1.5-EOF-0	595	29.4	0.7	19.5	0.7	0	13.2	1.04
D50×50×1.5-EOF-d1(30)	595	29.5	0.7	19.7	0.7	1346	13.8	1.02
D100×50×2.5-EOF-0	606	36.7	0.5	11.9	0.3	0	37.3	1.21
D100×50×2.5-EOF-d1(30)	606	36.9	0.5	11.9	0.3	2780	45.4	1.38
D100×50×2.5-EOF-d1(30)-R	606	36.8	0.5	11.9	0.3	2777	46.4	1.41
D80×40×2-EOF-0	606	36.0	1.0	15.0	0.4	0	16.1	0.92
D80×40×2-EOF-d1(30)	606	36.0	1.0	15.0	0.4	2160	18.3	0.95
D150×50×2.5-EOF-0	620	56.5	1.0	12.1	0.21	0	25.6	1.04
D150×50×2.5-EOF-d1(30)	620	56.7	1.0	12.2	0.21	4196	27.3	0.98
D100×100×1.8-EOF-0	606	51.6	1.0	16.7	0.3	0	14.0	0.98
D100×100×1.8-EOF-d1(30)	606	51.6	1.0	16.7	0.3	2784	18.5	1.11
D120×40×1.7-EOF-0	606	66.6	1.0	17.6	0.3	0	12.0	0.95
D120×40×1.7-EOF-d1(30)	606	66.6	1.0	17.6	0.3	3396	15.7	1.01
D150×150×1.8-EOF-0	606	79.3	1.0	16.7	0.2	0	14.1	1.03
D150×150×1.8-EOF-d1(30)	606	79.3	1.0	16.7	0.2	4284	18.1	1.05
D200×100×2-EOF-0	606	96.0	1.0	15.0	0.2	0	15.3	0.96
D200×100×2-EOF-d1(30)	606	96.0	1.0	15.0	0.2	5760	18.3	0.88
D200×50×1.7-EOF-0	606	113.6	1.0	17.6	0.2	0	11.5	0.97
D200×50×1.7-EOF-d1(30)	606	113.6	1.0	17.6	0.2	5796	14.0	0.83
Mean, P_m								1.04
COV, V_p								0.144
Reliability index, ß								2.51
Resistance factor, ϕ_w								0.85

Table 21: Web crippling test strengths verses predicted design strengths for lean duplex stainless steel specimens under EOF loading

Specimen	$f_{0.2}$ (MPa)	h/t	r_i/t	N/t	N/h	$A_{bonding}$ (mm)	P_{Exp} or P_{FEA} (kN)	$\frac{P_{Exp} \text{ or } P_{FEA}}{P_p}$
D50×50×1.5-IOF-0	595	29.2	0.6	32.3	1.1	0	19.6	0.81
D50×50×1.5-IOF-d1	595	29.4	0.7	32.7	1.1	2247	20.1	0.80
D100×50×2.5-IOF-0	606	36.8	0.5	19.9	0.5	0	60.5	1.06
D100×50×2.5-IOF-d1	606	36.8	0.5	19.9	0.5	4628	62.8	1.05
D100×50×2.5-IOF-d1-R	606	36.8	0.5	19.9	0.5	4633	63.2	1.06
D80×40×2-IOF-0	606	36.0	1.0	25.0	0.7	0	27.7	0.85
D80×40×2-IOF-d1	606	36.0	1.0	25.0	0.7	3600	30.5	0.87
D150×50×2.5-IOF-0	620	56.6	1.0	20.2	0.4	0	53.5	1.17
D150×50×2.5-IOF-d1	620	56.8	1.0	20.3	0.4	7003	55.0	1.10
D100×100×1.8-IOF-0	606	51.6	1.0	27.8	0.5	0	26.7	1.00
D100×100×1.8-IOF-d1	606	51.6	1.0	27.8	0.5	4640	31.5	1.06
D120×40×1.7-IOF-0	606	66.6	1.0	29.4	0.4	0	22.4	0.94
D120×40×1.7-IOF-d1	606	66.6	1.0	29.4	0.4	5660	26.7	0.98
D150×150×1.8-IOF-0	606	79.3	1.0	27.8	0.4	0	29.3	1.14
D150×150×1.8-IOF-d1	606	79.3	1.0	27.8	0.4	7140	33.9	1.13
D200×100×2-IOF-0	606	96.0	1.0	25.0	0.3	0	30.8	1.03
D200×100×2-IOF-d1	606	96.0	1.0	25.0	0.3	9600	34.9	0.98
D200×50×1.7-IOF-0	606	113.6	1.0	29.4	0.3	0	23.5	1.05
D200×50×1.7-IOF-d1	606	113.6	1.0	29.4	0.3	9660	27.8	0.98
Mean, P_m								1.00
COV, V_p								0.108
Reliability index, ß								2.56
Resistance factor, ϕ_w								0.85

Table 22: Web crippling test strengths verses predicted design strengths for lean duplex stainless steel specimens under IOF loading

Support and flange conditions	Load cases		C	C_R	C_N	C_h	$C_{ad\text{-}FRP}$	LRFD ϕ_w	Types
Unfastened Stiffened or partially stiffened flanges	Two-flange loading	ETF	3.3	0.32	0.49	0.020	0.025	0.85	Ferritic stainless steel
		ITF	5.4	0.26	0.48	0.001	0.040	0.85	
	One-flange loading	EOF	3.6	0.12	0.45	0.020	0.040	0.85	
		IOF	10.0	0.23	0.17	0.010	0.025	0.85	
	Two-flange loading	ETF	3.5	0.32	0.50	0.04	0.020	0.80	Lean duplex stainless steel
		ITF	5.5	0.26	0.51	0.01	0.030	0.85	
	One-flange loading	EOF	4.7	0.40	0.49	0.02	0.035	0.85	
		IOF	7.2	0.40	0.51	0.02	0.025	0.85	

Notes: The limitation of coefficients for: (i) ferritic stainless steel sections $4.8 \leq h/t \leq 107$, $N/t \leq 31$, $N/h \leq 2.6$ and $\theta = 90^o$; (ii) lean duplex stainless steel sections, $7.1 \leq h/t \leq 113.6$., $N/t \leq 32.8$, $N/h \leq 2.4$ and $\theta = 90^o$.

Table 23: Coefficients for proposed web crippling design equation of CFRP-strengthened stainless steel tubular sections under different loading configurations